Thesis

Two-Dimensional Electron Systems in Inhomogeneous Magnetic Field Environment

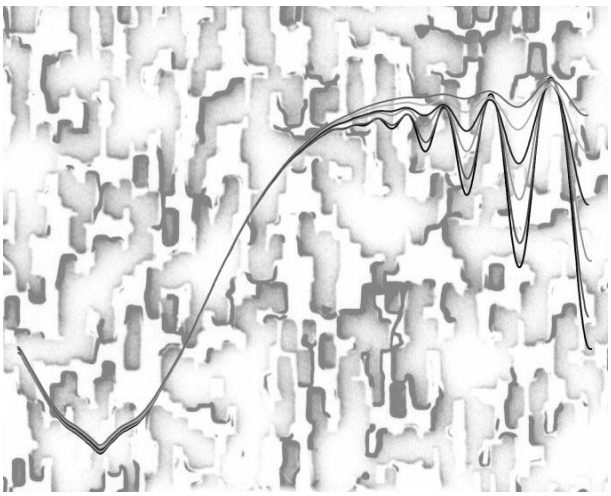

Masato Ando

Department of Physics, Graduate School of Science
The University of Tokyo
and
Institute for Solid State Physics
The University of Tokyo

December 2000

Preface

Two-dimensional systems are often of great interest in condensed matter physics because of its dimensionality. Phenomena that are unique to two-dimensional electron systems include quantum Hall effect, marginality of Anderson localization, high-T_c superconductivity, which are all based on the dimension *two*. Two-dimensional space is also peculiar in that a magnetic field effectively becomes a scalar field with its perpendicular component. This allows one to treat scalar potential and magnetic field on a similar basis.

This study is an experimental attempt to explore the two-dimensional electron system in modulated magnetic fields. Field modulation includes two-dimensinal as well as one-dimensional ones, with focus on two-dimensional random modulation. The papar is organized as follows. In Chapter 1, theoretical and experimental backgrounds of the two-dimensional system and modulated magnetic fields are reviewed. In Chapter 2, the design of our experiment and the procedure of sample preparation and measurement is described. We present our experimental results and discussion in Chapter 3. Concluding remarks are given in Chapter 4.

Part of the contents of this thesis is published as Reference [1].

Title page picture: Magnetoresistance of a two-dimensional electron system in the presence of a random magnetic field and a scanning electron micrograph of the sample V17303, used for the measurement.

Contents

List of Symbols and Abbreviations

$e\ (>0)$	Unit charge (electron charge is $-e$)
m_e	Bare electron mass
m^*	Effective mass of electron
n_e	Carrier density
ε_{F}	Fermi energy
k_{F}	Fermi wave number
$v_{\mathrm{F}} = \hbar k_{\mathrm{F}}/m^*$	Fermi group velocity
τ	Transport scattering time
τ_{tot}	Total scattering time
$l = v_{\mathrm{F}}\tau$	Mean free path
$\mu = e\tau/m^*$	Transport mobility
B	Magnetic field
$\phi_0 = h/e$	Flux quantum ($h/2e$ for superconductor)
$l_B = \sqrt{\hbar/eB}$	Magnetic length
$R_{\mathrm{c}} = \hbar k_{\mathrm{F}}/eB$	Cyclotron radius at the Fermi surface
$\boldsymbol{r} = (x, y)$	Spatial coordinate in the two-dimensional plane
$B(\boldsymbol{r}) = \bar{B} + \delta B(\boldsymbol{r})$	z-component of local magnetic field
$\bar{B}$	Uniform component of the magnetic field
$\delta B(\boldsymbol{r})$	Modulation component of the magnetic field ($\langle \delta B(\boldsymbol{r}) \rangle = 0$)

a	Modulation period for one-dimensional modulation
$K = 2\pi/a$	Modulation wave vector
ξ_B	Field correlation length ($\langle \delta B(\boldsymbol{r}) \delta B(\boldsymbol{r'}) \rangle \propto \exp[-\lvert \boldsymbol{r} - \boldsymbol{r'} \rvert / \xi_B]$)
$B_\parallel$	External in-plane field
$B_\perp$	External perpendicular field
ϕ	Azimuthal angle of $B_\parallel$ from the x-axis
1D	One-dimension[al]
2D	Two-dimension[al]
2DES	Two-dimensional electron system
MMF	Modulated magnetic field
RMF	Random magnetic field

Chapter 1

Introduction

In this chapter, we overview the theoretical and experimental backgrounds related to our topic. In Sec.1.1 we introduce the two-dimensional electron system and its basic properties in a uniform magnetic field. In Sec.1.2 systems with field modulation (magnetic, as well as electric) in only one direction are reviewed. These systems are often referred to as Weiss system and their transport property are understood with good quantitative accuracy. In Sec.1.3 we review the systems with two-dimensional (2D) field modulation, not including random magnetic field. These systems are understood far less than those with one-dimensional (1D) modulations. Detailed description on the issues of the random magnetic field will appear later in Sec.1.4.

1.1 Two-dimensional electron system

Two-dimensional electron system (2DES) at semiconductor interface, particularly that at GaAs/AlGaAs heterointerface, has been the stage of various experiment in condensed matter physics. This relies on the fact that this system allows one to control or decorate an otherwise idealistic free electron gas. 2D electrons at GaAs/AlGaAs interface have the energy dispersion $\varepsilon(\boldsymbol{k}) = \hbar^2\boldsymbol{k}^2/2m^*$ and behave as free electrons with the effective mass $m^* = 0.067m_e$, where m_e is the bare electron mass. Recent development of molecular beam epitaxy (MBE) has realized an 2DES with a high mobility exceeding 10^3 m^2/Vs, which correspond to a mean free path as long as $l \approx 100$ μm. Carrier density and Fermi wave number of a typical GaAs/AlGaAs 2DES are $n_e \approx 2{\times}10^{15}$ m^{-2} and $k_{\rm F} \approx (10\text{ nm})^{-1}$, respectively.

Motion of 2DEG in magnetic field As an introduction to the topic of spatially modulated magnetic field, let us first overview the transport properties of 2DES in a uniform magnetic field. The motion of an electron in a magnetic field B is characterized with the cyclotron motion with the cyclotron frequency $\omega_{\rm c} = eB/m^*$. An electron occasionally experiences a scattering at the scattering rate τ^{-1} and diffuses away from the initial position. The cyclotron radius $R_{\rm c} = \hbar k_{\rm F}/eB$ of an electron at Fermi surface often comes into play when magnetotransport of a 2DES in modulated structures are concerned. Another relevant length scale, especially in the strong field limit, is the magnetic length $l_B = \sqrt{\hbar/eB}$, which is the unit span of the quantized cyclotron motion.

Boltzmann's equation of transport The semiclassical transport theory is based on the Boltzmann equation for the electron distribution function $f(\boldsymbol{r}, \boldsymbol{v}, t)$

$$\left\{ \boldsymbol{v}\frac{\partial f}{\partial \boldsymbol{r}} + \frac{1}{m^*}\left(-\frac{\partial V(\boldsymbol{r})}{\partial \boldsymbol{r}} - e\boldsymbol{v}\times\boldsymbol{B}(\boldsymbol{r}) \right)\cdot\frac{\partial f}{\partial \boldsymbol{v}} \right\} - \left(\frac{\partial f}{\partial t}\right)_{\rm coll} = \frac{e\boldsymbol{E}^{\rm ext}}{m}\cdot\frac{\partial f}{\partial \boldsymbol{v}}. \quad (1.1)$$

To consider the linear response to an external electric field $\boldsymbol{E}^{\rm ext}$ at $T = 0$, we may restrict the velocity to the Fermi velocity and introduce polar coordinate $\boldsymbol{v} = v\boldsymbol{e}_v = \langle v, \phi\rangle$, rewrite the equation for the deviation from the Fermi distribution $g(\boldsymbol{r}, \phi)\delta(v - v_{\rm F}) = f(\boldsymbol{r}, \boldsymbol{v}) - f_0$ as

$$\left[v_{\rm F}\boldsymbol{e}_v\cdot\frac{\partial}{\partial \boldsymbol{r}} + \omega_{\rm c}(\boldsymbol{r})\frac{\partial}{\partial\phi} \right] g(\boldsymbol{r},\phi) - \left(\frac{\partial g}{\partial t}\right)_{\rm coll} = \frac{-e\boldsymbol{E}^{\rm ext}}{m^*}\cdot\boldsymbol{e}_v, \quad (1.2)$$

where $\boldsymbol{e}_v = (\cos\phi, \sin\phi)$ is the unit vector parallel to $\boldsymbol{v}$ and $\omega_{\rm c}(\boldsymbol{r}) = eB(\boldsymbol{r})/m^*$ is the cyclotron frequency corresponding to the magnetic field $B(\boldsymbol{r})$. There are several models for the collision term $(\partial g/\partial t)_{\rm coll}$ but the simple relaxation form $(\partial g/\partial t)_{\rm coll} = -g/\tau$ is often used. For a uniform system, the above assumption leads straightforwardly to the well-known Drude formula of conductivity σ and resistivity ρ

$$\sigma = \frac{\sigma_0}{1+(\omega_{\rm c}\tau)^2}\begin{pmatrix} 1 & +\omega_{\rm c}\tau \\ -\omega_{\rm c}\tau & 1 \end{pmatrix}, \quad \sigma_0 = \frac{n_e e^2\tau}{m^*} \quad (1.3)$$

$$\rho = \rho_0\begin{pmatrix} 1 & -\omega_{\rm c}\tau \\ +\omega_{\rm c}\tau & 1 \end{pmatrix}, \quad \rho_0 = \sigma_0^{-1}. \quad (1.4)$$

Landau level and quantum Hall effect When the magnetic field becomes sufficiently strong ($\omega_c\tau \geq 1$), one has to take into account the quantization of the cyclotron motion. The quantized energy levels are called Landau levels. For a free electron without any scatterers, the energy eigenvalue and eigenfunction in the Landau gauge $\boldsymbol{A}(\boldsymbol{r}) = (0, Bx, 0)$ are

$$\varepsilon_{N,ky} = \left(N + \frac{1}{2}\right)\hbar\omega_c \quad , \quad N = 0, 1, 2, 3, \cdots \tag{1.5}$$

$$\psi_{N,ky}(x, y) = \frac{\mathrm{e}^{ik_y y}}{\sqrt{L_y}}\phi_N(x + l_B^2 k_y), \tag{1.6}$$

where $\phi_N(x)$ is the N-th eigenstate of a harmonic oscillator with frequency ω_c. In the presence of impurity potential, each Landau level broadens to a width $\Gamma \simeq \hbar/\tau$.

As the magnetic field becomes strong and the peak structure of the Landau level's density of state becomes eminent, the magnetoresistance of the 2DES exhibits the Shubnikov-de Haas (SdH) oscillation periodic in B^{-1} with the period $\Delta(1/B)_{\mathrm{SdH}} = 2e/n_e h$. In the strong field limit, the 2DES enters the quantum Hall states where its resistance is expressed as

$$\rho = \begin{pmatrix} 0 & -\frac{1}{\nu}\frac{h}{e^2} \\ +\frac{1}{\nu}\frac{h}{e^2} & 0 \end{pmatrix}, \tag{1.7}$$

with filling factor ν being an integer (integer quantum Hall effect : IQHE) or odd-denominator fractional number (fractional quantum Hall effect : FQHE).

1.2 One-dimensional modulation

1.2.1 Electric and magnetic Weiss oscillation

The first successful experimental studies on 2DES under spatially modulated magnetic field have been reported in 1995. As these studies on 2DES under one-dimensional (1D) modulated magnetic field (MMF) were strongly inspired by the study on system with their electrostatic potential (electric field) modulation counterpart, we first take a brief look at the potential modulation and then come back to magnetic field modulation.

Electric Weiss oscillation In 1989, Weiss *et al.* [2, 3] and Winkler *et al.* [4] have found a novel oscillation in magnetoresistance of a 2DES under periodic electrostatic potential modulation with period $a \approx 500$nm

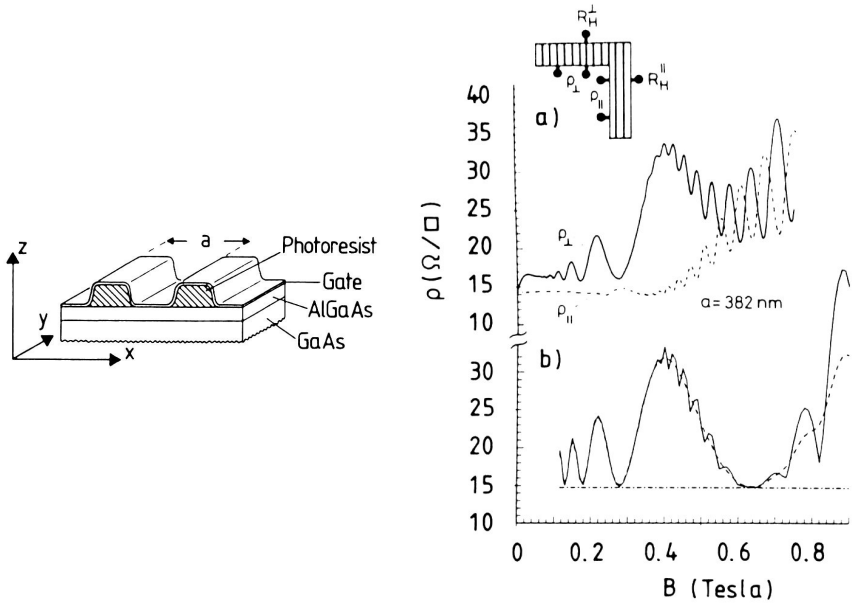

Figure 1.1: Left: Illustration of the sample structure for Weiss oscillation. Taken from Ref. [4]. Right: Observed magnetoresistance oscillation, compared with calculation. Taken from Ref. [3].

(Fig.1.1). The novel oscillation was periodic in $1/B$ with a period different from the Shubnikov-de Haas oscillation.

The explanation of this magnetoresistance oscillation was soon given as a commensurability oscillation of the modulation period a with the cyclotron radius $R_{\rm c} = \hbar k_{\rm F}/eB = k_{\rm F} l_B^2$ of an electron at the Fermi surface. The minima of ρ_{xx} occurs at the magnetic field values that satisfy

$$\frac{2R_{\rm c}}{a} = n - \frac{1}{4}, \tag{1.8}$$

with integer n. This condition is obtained as follows. Let us approximate the periodic potential with its first Fourier component

$$V(x) = \delta V \cos(Kx). \tag{1.9}$$

This potential lifts the degeneracy of the Landau level (1.5) and gives rise to a k_y-dependent dispersion of the energy eigenvalue, which leads to a non-trivial drift velocity along the y-axis. The dispersion of the energy eigenvalue and the drift velocity evaluated within first order perturbation are

$$\varepsilon^{(1)}_{N,k_y} = \langle N, k_y | V(x) | N, k_y \rangle = \delta V \, F_N(u) \cos(KX) \tag{1.10}$$

$$v_y = \frac{1}{\hbar}\frac{\partial \varepsilon^{(1)}_{N,k_y}}{\partial k_y} = \frac{K\delta V}{eB} F_N(u)\sin(KX), \tag{1.11}$$

respectively, where $X = -l_B^2 k_y$, $u = K^2 l_B^2/2$, and $F_N(u) = \mathrm{e}^{-u/2}L_N(u)$ with $L_N(u)$ being the Laguerre polynomial of N-th order. This gives rise to additional contribution to the yy-component of the conductivity proportional to its r.m.s. value on the Fermi level:

$$\Delta\sigma_{yy} = \frac{2e^2\tau}{2\pi l_B^2 \hbar\omega_\mathrm{c}} \langle (\bar{v}_y^{\mathrm{drift}})^2 \rangle_{\mathrm{Fermi}}, \tag{1.12}$$

while its contribution to other components are small. Since $\sigma_{xy}^2 \gg \sigma_{xx}\sigma_{yy}$ in the magnetic field range where the oscillation is observed, $\rho_{xx} = \sigma_{yy}/(\sigma_{xx}\sigma_{yy} + \sigma_{xy}^2) \approx \sigma_{yy}/\sigma_{xy}^2$, the minima of ρ_{xx} coincides with the minima of σ_{yy}. One can understand that minima of the σ_{yy} occurs when the width of the Landau subband is minimal. To obtain the condition (1.8), let us replace the Landau index N at the Fermi level with $\varepsilon_\mathrm{F}/\hbar\omega_\mathrm{c}$ and employ the asymptotic expression for $L_N(u)$ to get

$$F_N(u) \to \sqrt{\frac{2}{\pi K R_\mathrm{c}}} \cos\left(KR_\mathrm{c} - \frac{\pi}{4}\right), \tag{1.13}$$

which are also good approximations in this field range. The zeros of this expression is expressed with (1.8).

An alternative explanation is given by Beenakker [5]. For a weak modulation, the motion of an electron can be approximated with a cyclotron orbit, with the guiding center (X, Y) drifting with the drift velocity

$$\boldsymbol{v}^{\mathrm{drift}}(\boldsymbol{r}) = \frac{\boldsymbol{E}(\boldsymbol{r}) \times \boldsymbol{B}}{B^2} \tag{1.14}$$

at the local position $\boldsymbol{r} = (X + R_\mathrm{c}\cos\omega_\mathrm{c}t, Y + R_\mathrm{c}\sin\omega_\mathrm{c}t)$ along the cyclotron orbit. The local electric field is $(-e)E_x = -dV(x)/dx = K\delta V \sin(Kx)$, and therefore the drift velocity is along the y-axis. Its time average $\bar{v}_y^{\mathrm{drift}}$ is obtained by integrating the electric field along the orbit,

$$\begin{aligned} \bar{v}_y^{\mathrm{drift}} &= \frac{1}{2\pi B}\int_0^{2\pi} d\phi\, K\delta V\, \sin\left[K(X + R_\mathrm{c}\sin\phi)\right] \\ &= \frac{K\delta V}{eB} J_0(KR_\mathrm{c})\sin(KX), \end{aligned} \tag{1.15}$$

where J_0 is the Bessel function of the 0-th order. This gives the same asymptotic form as (1.11), and leads to the same condition (1.8). Functional form of magnetoresistance was studied in detail by Vasilopoulus and Peeters [6, 7].

Magnetic Weiss oscillation The magnetic field version of the Weiss oscillation was soon examined by some theories [8–10], which predicted a similar oscillation in the magnetoresistance for a 2DES with modulated magnetic field (MMF) as for electrostatic potential modulation, but with the condition of the resistance minima being

$$\frac{2R_{\rm c}}{a} = n + \frac{1}{4}, \tag{1.16}$$

instead of (1.8). This condition can be obtained by considering a sinusoidal MMF *

$$B(\boldsymbol{r}) = \bar{B} + \delta B \cos(Kx) \tag{1.17}$$

and performing a similar calculation of energy dispersion and drift velocity, to first order in δB:

$$\varepsilon^{(1)}_{N,k_y} = \hbar\delta\omega_{\rm c} G_N(u)\cos(KX) \tag{1.18}$$

$$v_y = \frac{1}{\hbar}\frac{\partial\varepsilon^{(1)}_{N,k_y}}{\partial k_y} = Kl_B^2\delta\omega_{\rm c}\, G_N(u)\cos(KX), \tag{1.19}$$

where $\delta\omega_{\rm c} = e\delta B/m^*$. Asymptotic form for $G_N(u)$

$$\begin{aligned} G_N(u) &= e^{-u/2}\left[\frac{L_N(u)}{2} + L^1_{N-1}(u)\right] \\ &\to -\frac{k_{\rm F}}{K}\sqrt{\frac{2}{\pi K R_{\rm c}}}\sin\left(KR_{\rm c} - \frac{\pi}{4}\right) \end{aligned} \tag{1.20}$$

gives the condition (1.16).

Successful observations of the magnetic Weiss oscillation were reported in 1995 by three different groups [11–13]. Fig.1.2 shows the experimental results of Izawa *et al.* [11], who used nickel stripes to produce the periodic field. The external magnetic field magnetizes the micropatterned nickel stripes on the 2DES Hall bar and produces a MMF on top of a uniform field.

Let us point out that the early studies on magnetic field modulation encounterd an experimental obstacle that the metal strips on the 2DES specimen produced a strain-induced potential modulation on the 2DES. In the work cited earlier [11], a gate bias applied on the nickel stripe is used to counteract this strain-induced potential. It has recently been shown that the strain-induced potential is mostly due to the piezoelectric coupling, and that it can be minimized by setting the direction of the modulation parallel to the [100] crystallographic direction [14].

*Throughout this thesis, we use the expression $B(\boldsymbol{r})$ for the z-component of the total magnetic field at $\boldsymbol{r}$, $\bar{B} = \langle B(\boldsymbol{r})\rangle$ for its spatial average, and δB for the modulation component with zero-average.

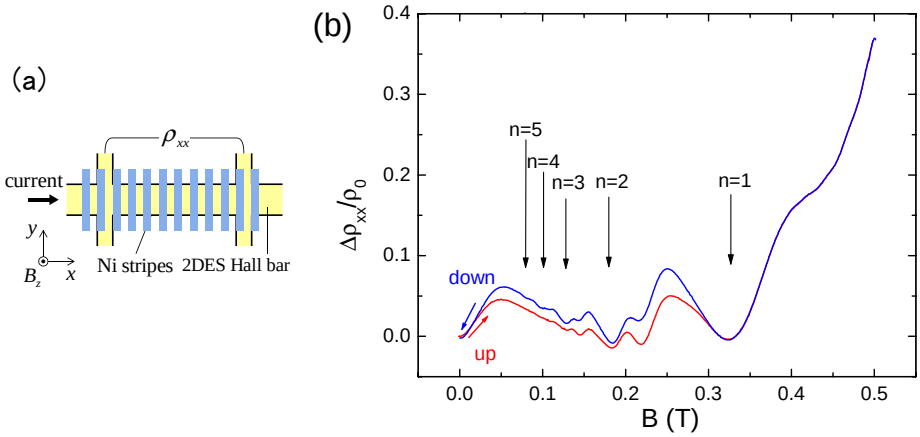

Figure 1.2: (a) Schematic of the sample for 1D MMF. (b) Observed magnetoresistance. The arrows indicate the expected positions of the resistivity minima. Taken from Ref. [11].

Low-field positive magnetoresistance Magnetic Weiss oscillation was a phenomenon observed in a situation where uniform magnetic field $\bar{B}$ as well as modulated magnetic field $\delta B(\boldsymbol{r})$ is present. $\delta B(\boldsymbol{r})$ was treated as a small perturbation to the Landau levels defined by $\bar{B}$. The regime where the modulated component $\delta B(\boldsymbol{r})$ dominates the transport properties of the 2DES has recently become a topic of some studies.

The magnetoresistance of a magnetic Weiss system shows a clear positive curve at the low field. A study on this low-field positive magnetoresistance is performed by Nogaret *et al* [15]. The low-field transport was described in terms of a so-called "snake orbit" that propagates in the y-direction along zero-magnetic field contours (Fig.1.3). The positive magnetoresistance is considered to arise from an enhanced diffusion in the y-direction, which recalls the mechanism of Weiss oscillation but of different nature.

1.2.2 Resistivity from electron-electron scattering in zero-mean modulation

When the external magnetic field is applied parallel to the 2D plane of a sample used in the study of magnetic Weiss oscillation, the magnetic material is magnetized parallel to the 2D plane and the fringing fields form a periodic MMF with zero-mean (Fig.1.4). This gives rise to a profound effect on the temperature dependence of 2DES resistivity.

The temperature dependence of the resistivity in semiconductor 2DES

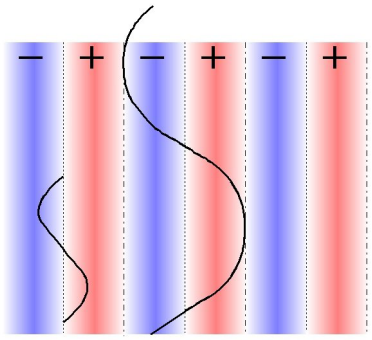

Figure 1.3: Snake orbits that travels along the $B = 0$ contour of the MMF.

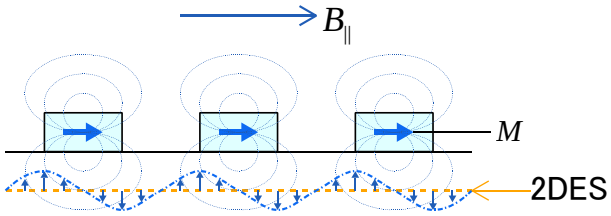

Figure 1.4: Schematic drawing of the magnetic field profile when the external field is applied parallel to the 2DES plane.

were studied intensively in the '80s. The low-temperature resistance of a high-mobility 2DES is dominated by a residual resistivity from remote impurity scattering that is constant of the temperature T, plus a T-linear term from acoustic phonon scattering [16, 17]. Electron-electron (e-e) scattering, which plays an essential role in the energy relaxation within an electron system, does not contribute to resistivity because it preserves the total momentum in a translationally-invariant system.

When some kind of field modulation is introduced to such system, umklapp process that alters the total momentum becomes possible and gives rise to a resistivity component from e-e scattering. This issue is recently addressed by Messica *et al.* [18] for electrostatic modulation, followed by Overend *et al.* [19] and Kato *et al.* [20] for magnetic field modulaiton. They created a zero-mean MMF by applying a in-plane external field to their 1D MMF sample and observed a T^2-dependent resistivity component in the 2DES when MMF is present (Fig.1.5).

Theoretically, the temperature dependence of e-e scattering rate at the

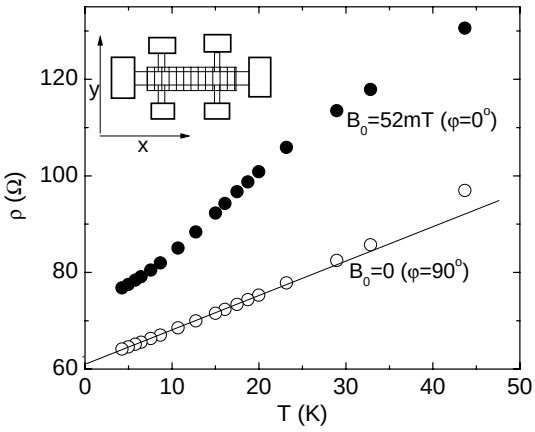

Figure 1.5: The resistivity of a 2DES in the presence (B_0 = 52mT) and absence (B_0=0) of MMF. The former has a T^2-component which is not found in the latter. Taken from Ref. [20].

Fermi level is given as

$$\frac{1}{\tau_{\rm ee}} \propto T^2 \ln\left(\frac{\varepsilon_{\rm F}}{k_{\rm B}T}\right) \tag{1.21}$$

for two-dimension. We may expect the resistivity component from e-e umklapp scattering to have the same temperature dependence. Recently Sasaki *et al.* [21] have studied the conductivity of a 2DES in a specific case where weak periodic magnetic field $\delta B(\boldsymbol{r}) = \delta B \cos(Kx)$ is present. They yielded the correction due to the periodic field as

$$\begin{aligned} -\Delta\sigma &= \frac{e^2}{h}(\delta\omega_{\rm c}\tau)^2 \frac{\sqrt{k_{\rm F}^2 - (K/2)^2}}{K} \\ &+ \frac{\pi^2}{6}\frac{e^2}{h}(UD)^2 \left(\frac{k_{\rm F}}{K}\right)^2 (\delta\omega_{\rm c}\tau)^2 \frac{\tau}{\hbar}\frac{(k_{\rm B}T)^2}{\varepsilon_{\rm F}}, \end{aligned} \tag{1.22}$$

where U is the strength of the e-e interaction and D is the density of states at the Fermi level. The first term is constant of T and the second term gives the T^2-contribution. Kato *et al.* [20] have compared their experimental data with this expression and obtained a reasonable agreement.

1.3 Two-dimensional modulation

Behavior of 2DES in 2D modulation is understood far less than its 1D counterpart, because of its complexity. The simplest 2D modulation consists

of two Fourier components and in many cases two-wave approximation does not describe experimental systems well. In addition, analytical treatment of 1D modulation imposed on uniform background field was specifically facilitated by taking the Landau gauge, in which unperturbed wave fuction can be taken plane wave in one direction.

The energy spectrum of electron in 2D potential modulatino shows an intricate fractal structure called Hofstadter's butterfly [22]. Some theoritical studies on 2D MMF discusses the energy spectra in such systems and show that there are similar fractal structure also for magnetic modulations [23–25]. However observation of such structures in semiconductor 2DES has not been reported so far because they are easily smeared out by temperature and the lifetime broadening of the electron.

Yoshida *et al.* [26] have studied numerically the magnetotransport of 2DES in a 2D MMF with classical billiard model and Kubo-type formula. They observed a commensurability peak in the magnetoresistance, which they attributed to the occurence of runaway orbits that skips between the periodic modulation (Fig.1.6).

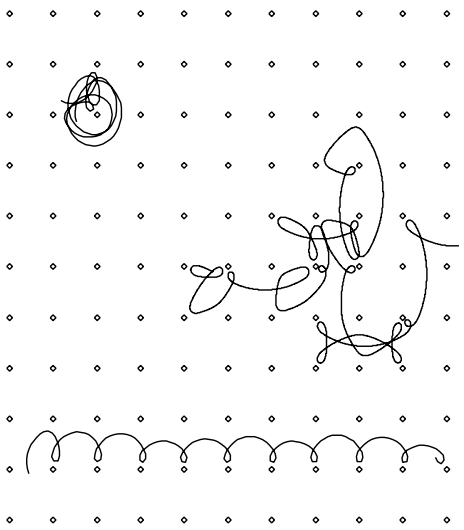

Figure 1.6: Typical three trajectories in 2D MMF imposed on uniform background field. Pinned, chaotic, and runaway orbits. Taken from Ref. [26].

To our knowledge, there is only a single experimental study published so far on semiconductor 2DES with 2D MMF. Ye *et al.* [27] deposited an 2D array of ferromagnetic dysprosium dots with period $a = 500$ nm on a 2DES Hallbar. The magnetoresistance showed a commensurability minima

at the positions expected for 1D MMF with the period $a = 500$ nm. They did not mention any behavior in the electron transport that reflects the dimensionality of the modulation.

1.4 Random magnetic field

Properties of 2DES in random magnetic field (RMF) has attracted particular interests among spatially modulated structures because of its relevance to some fundamental problems in the solid state physics. Those include the problem of localization [28–30], composite fermion model of half-filled Landau level [31–33], and gauge field theory of high-T_c superconductors [34]. Here we view some of these aspects of 2DES in RMF and theory of trasport in such system.

1.4.1 Relevance to localization

It is generally believed by now that, in two-dimension, all non-interacting electron states in random potentials are localized and 2DES are insulators in the limit of large system size and low temperature. This localization is of quantum nature in that the interference between time-reversal symmetric paths plays an essential role. Therefore, the localization is destroyed with uniform magnetic field which breaks the time-reversal symmetry. In contrast to the case of random *potential*, localization of 2DES in random *magnetic* field still remains a controversial issue. Many theoritical and numerical studies have been done on this problem.

Random flux model Among the models of RMF, random flux tight-binding model is probably the most intensively studied because of its simplicity. It is a modification of tight-binding model that the transfer integral t between lattice sites are twisted by random Peierls' phase $\theta_{i,j}$ (Fig.1.7). The Hamiltonian of this system can be written as

$$H = \sum_i \varepsilon_i + \sum_{\langle i,j \rangle} t e^{i\theta_{i,j}} c_i^\dagger c_j + \text{h.c.}, \tag{1.23}$$

where $\langle i, j \rangle$ indicates the nearest neighbors. The flux threading a plaquette is expressed as

$$\phi_{ijkl} = \frac{1}{2\pi} \frac{h}{e} \sum_{ijkl} \theta_{i,j}. \tag{1.24}$$

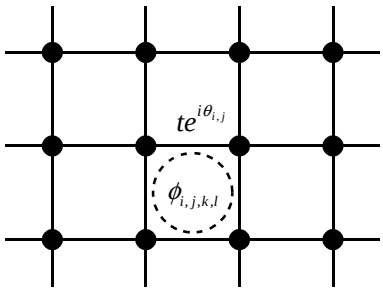

Figure 1.7: Schematic of the random flux model. Each transfer matrix element t is twisted by a random phase factor $\theta_{i,j}$.

The model is first considered by Lee and Fisher [28], and reexamined by a number of authors. Some of them concluded that all states are localized [29], but others argued that there exist some delocalized state(s) at the band center [30]. The extremely long localization length near the band center makes it difficult to draw a definite conclusion from the calculation in finite system.

Though the model deals with an RMF with much shorter correlation length and large modulation amplitude than our study, experiments may give a clue to this long-standing problem in the future.

1.4.2 Relevance to the composite fermion

Fractional quantum Hall effect A 2DES in a strong magnetic field enters quantum Hall (QH) states around some specific magnetic field values where the Landau level filling factor $\nu = n_e h/eB$ takes integer (intger QH effect : IQHE) or odd-denominator fractional (fractional QH effect : FQHE) values. The Hall resistivity ρ_{xy} takes the quantized value

$$\rho_{xy} = \frac{h}{e^2} \cdot \frac{1}{\nu}, \tag{1.25}$$

and the diagonal resistivity ρ_{xx} approaches zero.

While IQHE can be explained with a single electron picture that the Fermi level enters a mobility gap between Landau levels, FQHE is a many-body effect in its nature, as characterized by the Laughlin's many-body wave function [35]. There were some difficulty in constructing an appropriate wave function for hieralhical FQH states such as $\nu = n/(2n \pm 1)$. There was also an enigma concerning the filling factor $\nu = 1/2$, where ρ_{xx} shows a minimum like a QHE but was not likely to be a QH state because the Hall

resistivity ρ_{xy} does not form a plateau and the $\nu = 1/2$ minimum in ρ_{xx} does not develop towards the low temperature unlike the QH minima.

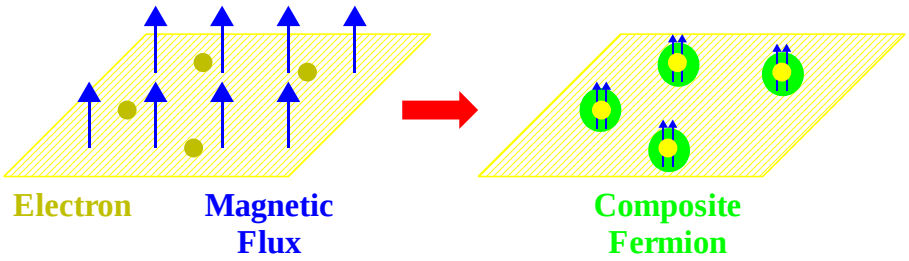

Figure 1.8: Schematic illustration of composite fermion. The CF feels the statistical field that cancels the external field at Half filling.

Composite fermion picture The composite fermion (CF) theory proposed by Jain [36] gave large clue to these problems. In this theory, the 2DES in strong magnetic field is described in terms of a fictutious particle named composite fermion, which consists of an electron and two magnetic flux quanta $\phi_0 = h/e$ (Fig.1.8). As a result of the flux attatchment, a CF feels a fictitious "magnetic" field

$$b = \nabla \times \boldsymbol{a} = -2\phi_0 n_e \tag{1.26}$$

proportional to the electron density n_e in addition to the external field B. When treated in the mean-field approximation, the the FQH states of the primary sequence $\nu = n/(2n \pm 1)$ are mapped to IQH states $\pm n$ of the CF, and the $\nu = 1/2$ state is mapped to the zero-field state of the CF.

Composite Fermion and RMF Despite the elegant mapping of the CF theory, there remain some subtle differences between the states around $\nu = 1/2$ and the true $B = 0$. One is the positive magnetoresistance as exemplified by the experiment by Jiang *et al.* (Fig.1.9 [37]), and another is the enhancement of the effective mass m^*_{CF} argued experimentally by Du *et al.* [38, 39] and theoritically by Halperin, Lee, and Read [40].

These differences are considered to occur from the physics omitted in the mean-field approximation – the fluctuation of the effective magnetic field, which means *random magnetic field*. It stems from the fluctuation of the local electron density $n_e(\boldsymbol{r})$. At $\nu = 1/2$, the effective magnetic field felt by a CF is

$$B_{\mathrm{eff}}(\boldsymbol{r}) = B + b(\boldsymbol{r}) = 2\left(n_e - n_e(\boldsymbol{r})\right)\phi_0 = -2\delta n_e(\boldsymbol{r})\phi_0, \tag{1.27}$$

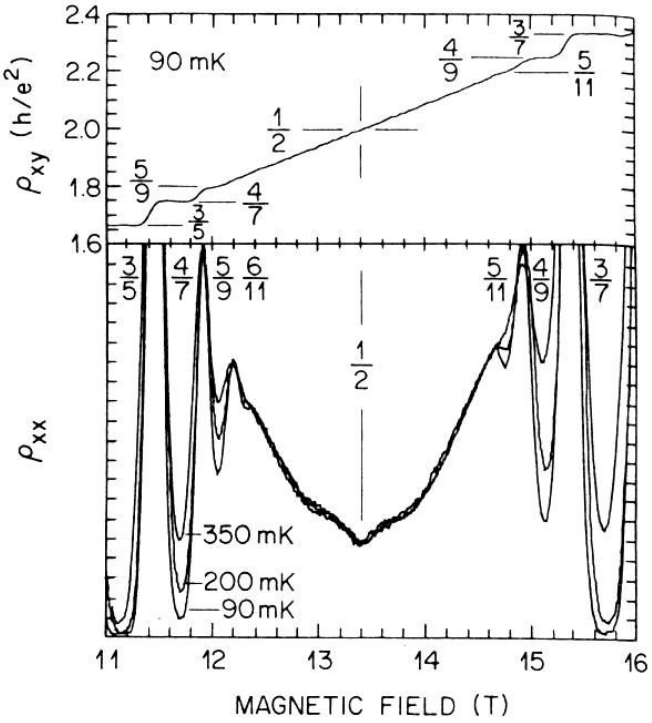

Figure 1.9: Hall- and longitudinal resistivity of a very-high mobility 2DES around $\nu = 1/2$. ρ_{xx} shows a minimum with characteristic structure that does not depend on the temperature as other FQH minima. Taken from Ref. [37]

where $\delta n_e(\boldsymbol{r}) = n_e(\boldsymbol{r}) - n_e$ is the local fluctuation of the electron density from its average value.

We should note that there are two kinds of RMF present in CF systems. Kalmeyer and Zhang [31] discussed that the random impurity potential induces a static inhomogeniety in the local electron density $\delta n_e(\boldsymbol{r})$ and leads to a static RMF $\delta B(\boldsymbol{r})$. The positive magnetoresistance around $\nu = 1/2$ is due to this effective RMF in their argument. The other source of the fluctuation is the electron correlation. According to Halperin, Lee, and Read [40], this term leads to a effective mass renormalization that diverges toward the Fermi level at $\nu = 1/2$.

Here let us call them "static" and "dynamical" RMF, respectively. The RMF realized in our experiment contains the former component only.

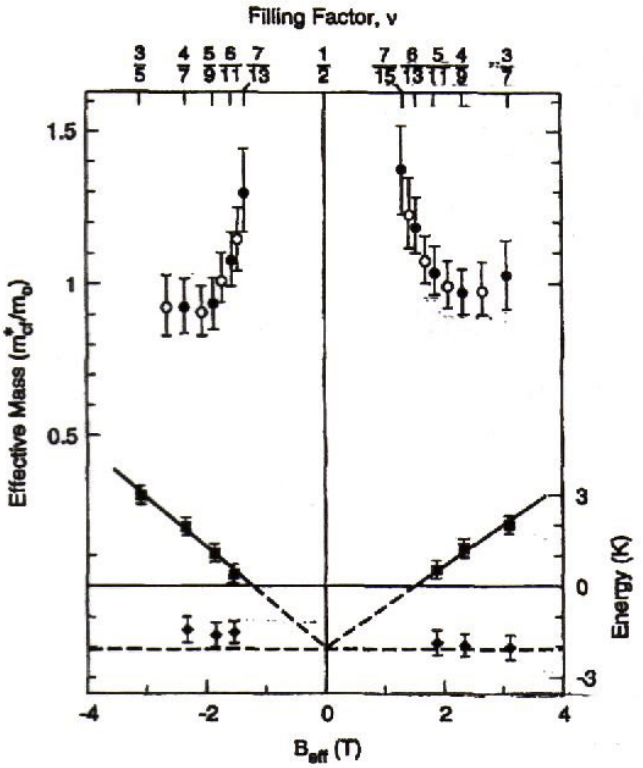

Figure 1.10: Effective CF mass as determined from the temperature dependence of the Shubnikov-de Haas oscillations (top and left), and energy gap as determined from activation energy measurements (bottom and right). The evaluated CF effective mass is about an order larger than the GaAs band mass $m^* \approx 0.067m_e$ and seems to diverge toward the $\nu = 1/2$. Taken from Ref. [39].

1.4.3 Transport in random magnetic field

Despite the large interest in the issue, actual transport properties of 2DES in RMF – how the resistivity behaves with introduction of RMF – is yet to be established. One reason is the wide range of situations depending on the five characteristic scales that come into the problem: The amplitude $|\delta B|$ and the correlation length ξ_B of the RMF, and the mean free path l, the average cyclotron radius $\bar{R}_\mathrm{c} = \hbar k_\mathrm{F}/e\bar{B}$, and the Fermi wavelength $2\pi/k_\mathrm{F}$ of the electron.

There are theoretical studies discussing the transport of 2DES in RMF in terms of quantum weak localization effect [41,42], and classical motion in the absence of potential scattering [43,44], focusing on different regimes of the five parameters. Here we follow the theory by Hedegård and Smith [45] which is consider to cover the experimental situation of our study.

The theory is based on semiclassical Boltzmann equation (1.2) and explicitly disregards weak localization effects. The RMF is treated as a random driving force while the ordinary impurity scattering is included in the collision term in the simple relaxation form. Putting the RMF in the driving-force term is justified when the correlation length ξ_B of the RMF is much greater than the Fermi wavelength: $k_\mathrm{F}\xi_B \gg 1$. The equation for the deviation $g(\boldsymbol{r}, \phi)$ from the Fermi distribution reads

$$\left\{ v_\mathrm{F}\boldsymbol{e}_v \cdot \frac{\partial}{\partial \boldsymbol{r}} + [\bar{\omega_\mathrm{c}} + \delta\omega_\mathrm{c}(\boldsymbol{r})] \frac{\partial}{\partial \phi} + \frac{1}{\tau} \right\} g(\boldsymbol{r}, \phi) = \frac{-e\boldsymbol{E}^\mathrm{ext}}{m^*} \cdot \boldsymbol{e}_v, \tag{1.28}$$

where $\boldsymbol{e}_v = (\cos\phi, \sin\phi)$, $\bar{\omega_\mathrm{c}} = e\bar{B}/m^*$, and $\delta\omega_\mathrm{c}(\boldsymbol{r}) = e\delta B(\boldsymbol{r})/m^*$. This can be rewritten as an operator equation

$$\mathcal{D}g \equiv (\mathcal{D}_0 + \mathcal{W})g = \chi \tag{1.29}$$

with the definitions

$$\mathcal{D}_0 = i\left\{ v_\mathrm{F}\boldsymbol{e}_v \cdot \frac{\partial}{\partial \boldsymbol{r}} + \bar{\omega_\mathrm{c}} \frac{\partial}{\partial \phi} + \frac{1}{\tau} \right\} \tag{1.30}$$

$$\mathcal{W} = i\delta\omega_\mathrm{c}(\boldsymbol{r}) \frac{\partial}{\partial \phi} \tag{1.31}$$

$$\chi(\boldsymbol{r}, \phi) = i\frac{-e\boldsymbol{E}^\mathrm{ext}}{m^*} \cdot \boldsymbol{e}_v. \tag{1.32}$$

The strategy is to find the Green function $\mathcal{G}$ for $\mathcal{D}$. Then we get

$$g(\boldsymbol{r}, \phi) = \int dr'^2 d\phi' \mathcal{G}(\boldsymbol{r}, \phi; \boldsymbol{r}', \phi')\chi(\boldsymbol{r}', \phi') \tag{1.33}$$

and the current density

$$\boldsymbol{j}(\boldsymbol{r}) = -2n_e e\frac{1}{2\pi}\int_0^{2\pi} d\phi \boldsymbol{e}_v g(\boldsymbol{r},\phi). \tag{1.34}$$

The Green function $\mathcal{G}$ is calculated with perturbative expansion from the Green function $\mathcal{G}_0$ for $\mathcal{D}_0$ in a manner similar to that for quantum mechanical Green function. The deviation from the Drude conductivity (1.4) is expressed in terms of "self energy" Σ of the averaged Green function $\mathcal{G} = (\mathcal{G}_0^{-1} + \Sigma)^{-1}$. $\Sigma = \langle \mathcal{W}\mathcal{G}_0\mathcal{W}\rangle$, evaluated to the second order in $\mathcal{W}$ contains the correlation function of the RMF

$$C_B(\boldsymbol{R}) = \langle \delta B(\boldsymbol{r})\delta B(\boldsymbol{r}+\boldsymbol{R})\rangle \tag{1.35}$$

which reflects the nature of the RMF.

The theory is applied to the experiments by Geim *et al.* [46], where the field modulation was caused by flux tubes. They assumed the correlation function of the form

$$C_B(\boldsymbol{R}) = \delta B^2 \exp\left(-\frac{R^2}{2\xi_B^2}\right) \tag{1.36}$$

and calculated the magnetoresistance. They also obtained the expression for the magnetoresistance

$$\frac{\Delta\rho_{xx}}{\rho_{xx}^0} = \left(\frac{\pi}{2}\right)^{1/2}\left(\frac{\xi_b}{l}\right)(\delta\omega_c\tau)^2 \coth\left(\frac{\pi}{\bar{\omega_c}\tau}\right) \tag{1.37}$$

for moderate fields and the limit $l/\xi_B \gg 1$. The overall shape of the magnetoresistance shown in Fig.1.11 is determined by the ratio $x = l/\xi_B$. The magnetoresistance crosses over from negative to positive as the correlation length ξ_B becomes much shorter then the mean free path l.

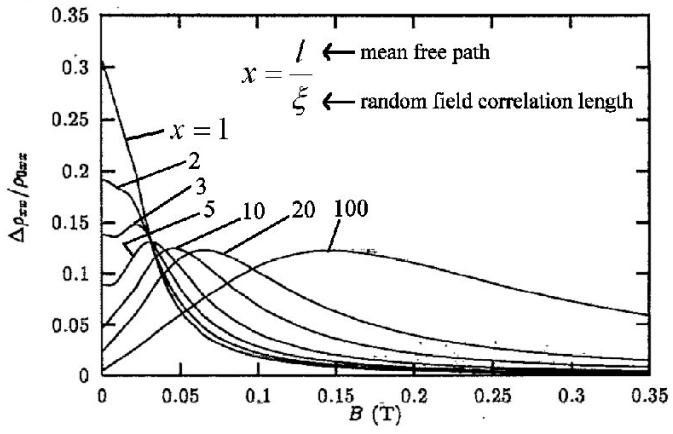

Figure 1.11: Relative change in longitudinal resistance of a 2DES in RMF with the correlation function (1.36). Parameters are $n_e = 4{\times}10^{15}$ m^{-2} and $\delta B = 10$ mT. l and ξ_B are varied such that $l\xi_B = (8.1\mu\text{m})^2$ to keep the curves on the same scale. Taken from Ref. [45]

Chapter 2

Design and Preparation of the Experimental System

The experimental procedure consists of sample preparation and measurement. However the most important step in the course of the experiment is the design of the whole system including the sample and the measurement setup. In Sec.2.1, we first discuss the design of the sample, that is, how to impose the modulated magnetic field onto the 2DES. Next in Sec.2.2, the preparation of the samples from raw 2DES wafers and the experimental setup for the measurement of magnetotransport is explained.

2.1 Design of the system

There are several methods to impose a modulated field on a 2DES. On designing such experimental systems, we have to take the following conditions into account.

1. The characteristic length scales relevant to the transport in 2DES are the mean free path $l = v_{\rm F}\tau = 1 \sim 10^3$ μm, Fermi wavelength $\lambda_{\rm F} = 2\pi/k_{\rm F} \approx 50$ nm, and the cyclotron radius $R_{\rm c} = k_{\rm F} l_B^2 \approx 70$ nm (at $B = 1$ T) of an electron at the Fermi level.

2. The 2DES is at the GaAs/GaAlAs heterointerface which is located typically about 100 nm away from the surface of the wafer.

3. For a clear discussion on the effect of the field modulation, it is essential to separate the uniform background component $\bar{B}$ and the pure modulation component $\delta B(\boldsymbol{r})$ of the magnetic field.

Let us take a brief look at the past experimental methods to produce modulated magnetic field (MMF). Geim *et al.* [46] deposited a uniform film of type-II superconductor on the top of 2DES wafer. An applied magnetic field creates the mixed state in the superconductor above the lower critical field B_{c1} and penetrates as distributed magnetic flux (vortices) with characteristic diameter close to the field penetration depth. The flux tubes tend to distributed randomly instead of forming the so-called Abrikosov lattice due to the inhomogeneity of the film (Fig.2.1 A). Smith *et al.* used small lead grains ranging from few to 80 microns and are randomly ditributed on the surface of the 2DES wafer [47]. The lead grains, which are type-I superconductor for these grain size, expells the magnetic field below critical field through the Meissner effect. The problem in using Meissner effect or mixed state of superconductor as a source of MMF is that they can produce only a small field modulation amplitude not more than the lower critical field.

Mancoff *et al.* [48, 49] attatched a macroscopic ($300\,\mu$m $\times$ 1.5 mm $\times$ $200\,\mu$m) slab of neodymium-iron-boron (NdFeB) ferromagnet on top of the 2DES Hall bar (Fig.2.1 C,D). The surface roughness with a lateral length scale of about 20 μm produces an inhomogeniety in the magnetic field felt by the 2DES. The field modulation amplitude is estimated to be as large as $\approx$100 mT. Rushforth *et al.* deposited on 2DES wafer a CoPd multilayer, which form a maze-like pattern of domain at certain points in the magnetization loop. The amplitude of the MMF prepared with these methods is fairly large but in these experiments the external field applied perpendicular to the 2D plane contributes to MMF as well as uniform background, which makes the analysis difficult.

Gusev *et al.* [50] took a unique approach. They prepared a nonplaner 2DES grown on a prepatterned substrate (Fig.2.1 B). By applying an external in-plane field, they were able to introduce an effective MMF. Since the external field is applied parallel to the 2D plane in this case, the average of the effective MMF is kept zero. However the mobility of the 2DES was greatly diminished from an ordinary 2DES, due to the difficulity in epitaxial growth process.

Probably the most popular method to produce MMF is to decorate the surface of a 2DES wafer with a pattened ferromagnets using microfabrication techniques. Ye [27, 51] deposited dysprosium dots regularly and randomly distributed on a 2DES Hall bar.

Patterned ferromagnets, when combined with a cross-coil system that allows one to impose two components of external field independently, enables us a systematic study particularly for 1D modulations. Kato *et al.* [20] have used this system to study electron-electron scattering process in 2DES

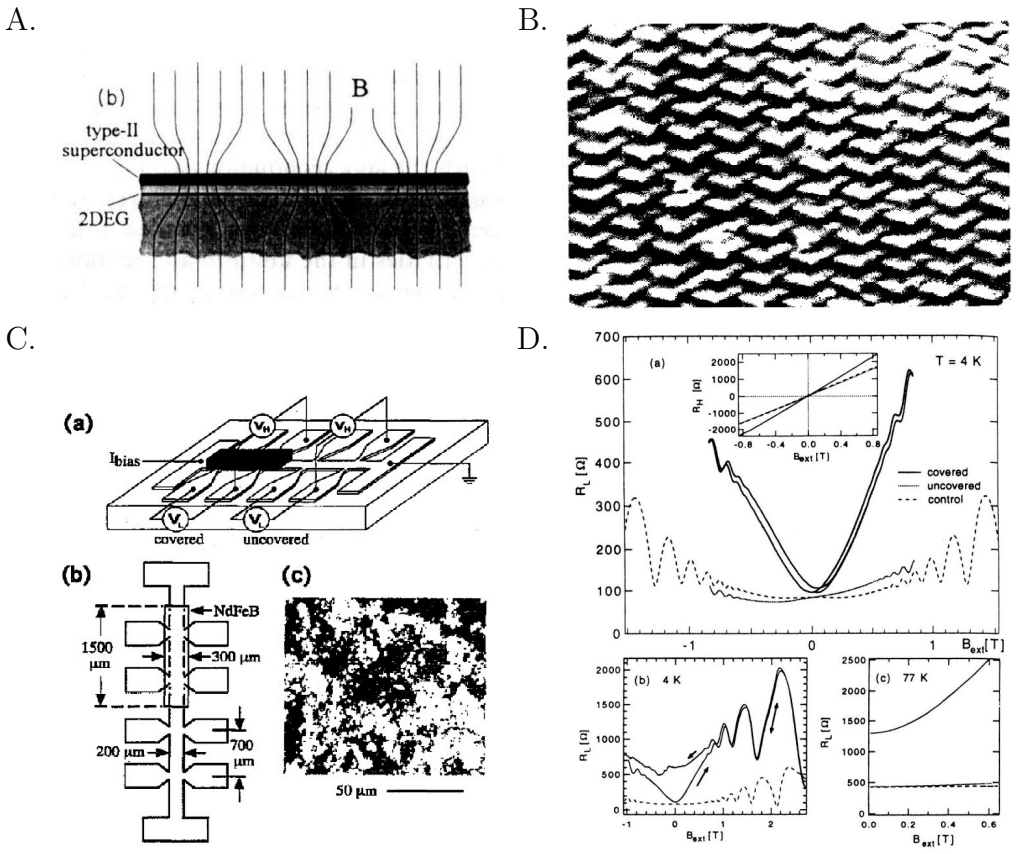

Figure 2.1: A. Schematic of 2DES-superconductor hybrid system. Taken from Ref. [46]. B. Plane-view scanning electron micrograph of a dimpled sample used in Ref. [50]. C. (a) Schematic, (b) Topview, and (c) Optical micrograph of the sample used in Refs [48] and [49]. D. (a) Longitudinal resistance vs external field measured under NdFeB magnet, compared with control sample. Strong positive magnetoresistance exists only for the covered case. The inset shows the Hall resistance. (b) for high-field scan, (c) at 77 K. Taken from Ref. [48].

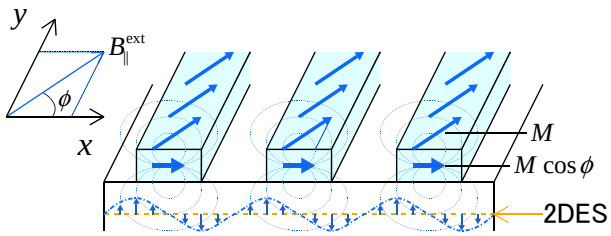

Figure 2.2: Schematic of patterned magnet for 1D MMF. The MMF amplitude δB can be controlled via the azimuthal angle ϕ of the in-plane field $B_{\parallel}$.

under 1D MMF. A strong external magnetic field $B_{\parallel}$ applied in-plane, with the angle ϕ from the modulation wave vector aligns the magnetization of the ferromagnetic stripes on the 2DES Hall bar and produces a zero-mean MMF (Fig.2.2). Because the system is uniform along the y-axis, the y-component M_y of the magnetization does not produce fringing field that threads the 2DES Hall bar. Thus the amplitude of the MMF is determined by the x-component as

$$|\delta B| \propto M_x = |\boldsymbol{M}| \cos\phi, \tag{2.1}$$

where $\boldsymbol{M}$ is the magnetization of the ferromagnet, which is well saturated at this external field. This means that $|\delta B|$ can be controlled via the azimuthal angle ϕ of $B_{\parallel}$ while the uniform field component $\bar{B}$ can be imposed independently with the other solenoid.

We should note that this method was particularly successful for 1D modulated system. For 2D modulations, we have to develop yet another scheme to gain a full control of $\bar{B}$ and $|\delta B|$. We have attempted two methods to achieve this, which is described in the following.

2.1.1 Patterned magnetic material

For most measurements, patterned ferromagnets are still a useful method for 2D modulations too. As long as cross-coil system is available, one can prepare a MMF of fixed amplitude by the in-plane field $B_{\parallel}$ and measure, for example, the magnetoresistance with respect to uniform field $\bar{B}$. However one encounters a difficulty when he attempts to control the amplitude $|\delta B|$ of the modulation, because the rotation of $B_{\parallel}$ now merely changes the pattern of the MMF in a complicated manner instead of the simple relation (2.1). For this purpose, we sought for another material whose magnetization is

1. not hysteretic so that the magnetization can be known as a single-valued function of the external field, so that $|\delta B|$ can be controlled via the strength of $B_{\parallel}$.

2. as large as ferromagnetic metals, in order to create a strong enough MMF on the 2DES plane.

Candidate material may be compounds of rare-earth metals such as Dy, Gd, which have large local magnetic moments at the inner shell. Since elementary substance of those $4f$ metals become ferromagnetic at low temperature and exhibit wide hysteresis loops, we attempted to kill the ferromagnetic order by introducing impurities. After some trial and error, it turned out that alloy of dysprosium with copper (DyCu) fulfills the above requirement.

Patterned film of DyCu is prepared by co-sputtering dysprosium with copper as shown in Fig.2.3. Copper content of the alloy can be varied with the number of 1 cm×1 cm copper chips placed on the 100 mmϕ dysprosium target.

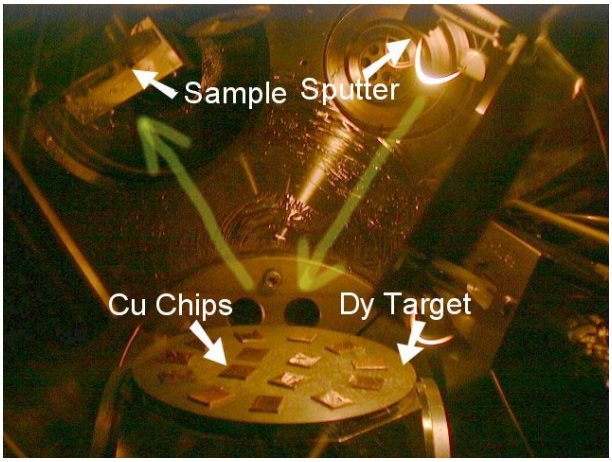

Figure 2.3: Inside the sputtering chamber when Dy (circle target) is co-sputtered with Cu (square chips). The sputtering ion beam is emitted from the source on the upper right in the picture towards the target at the bottom, evaporating the metal to the sample on the upper left.

An optical micrograph of one of the samples used in the study is shown in Fig.2.4. Figure 2.5 shows the magnetization curve of some DyCu films measured with a SQUID magnetometer, and compared with that of pure Dy film. The hysteresis loop of Dy is largely reduced by small amount of Cu and is almost closed at 4.2K for DyCu prepared with 30 Cu chips on the Dy target. The difference can be seen in the resistance of the 2DES. Fig.2.6

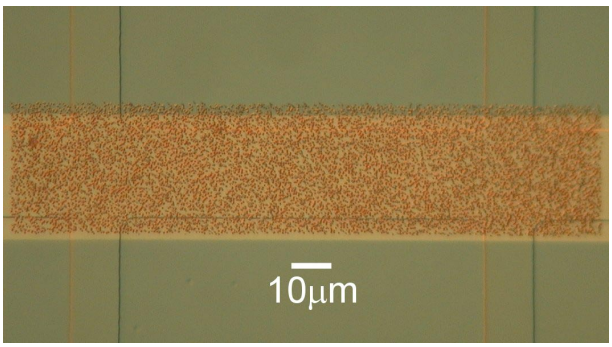

Figure 2.4: An optical micrograph of a sample for random magnetic field.

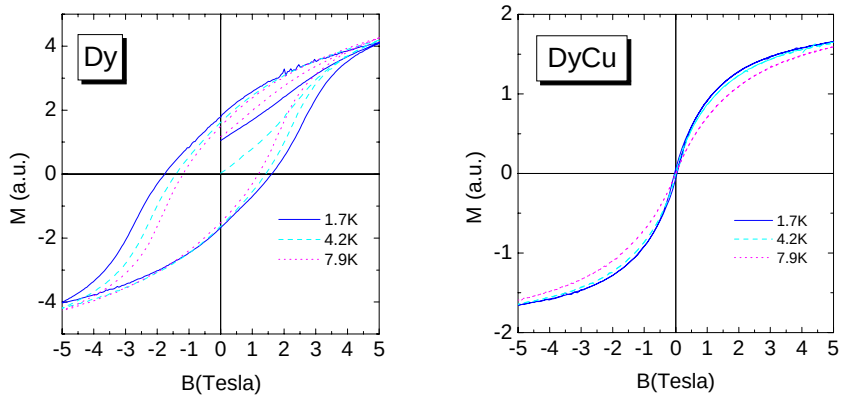

Figure 2.5: Magnetization of Dy (left) and DyCu (right). The large hysteresis loop of Dy is reduced by addition of Cu.

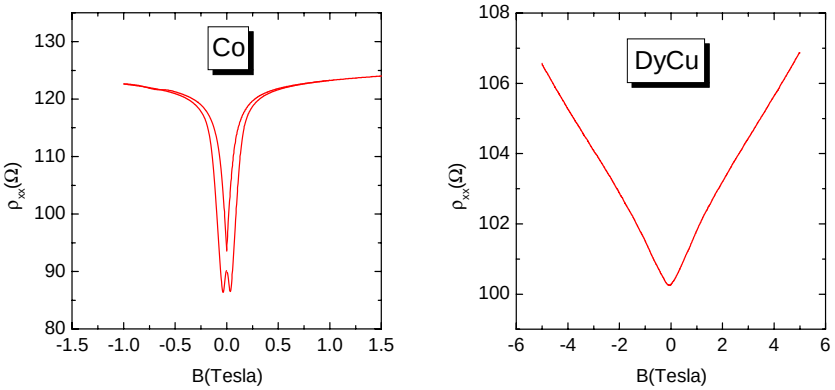

Figure 2.6: Resistance of 2DES with MMF by Co (left) and DyCu (right). The hysteresis of the magnetic layer is reflected to the resistivity of the 2DES.

shows the resistance of 2DES with patternd DyCu compared with a similar sample with cobalt. Most samples measured in this study use patterned Co or DyCu film for the MMF.

2.1.2 Superconducting meander coil

Another way to induce a magnetic field is to drive a current. Microscopic meander coil may be used to produce a MMF controllable with an external current. Considering that a current of 10 mA induces a magnetic field of 4 mT at a distance of 0.5 μm, it is possible to produce a MMF with an amplitude of few mT by driving a current through a micron-scale meander coil as shown in Fig.2.7. Ginzburg-Landau theory gives the critical current density for thin superconducting wire as

$$J_{\mathrm{c}} = \frac{cH_{\mathrm{c}}}{3\sqrt{6}\pi\lambda}, \tag{2.2}$$

where H_{c} is the critical field and λ is the penetration depth. This may exceed 100 mA/μm^2 for some niobium compounds such as NbTi, Nb_3Sn, or NbN, indicating the possibility to produce MMF with superconducting meander coils. These superconductors listed above survive the external magnetic field for transport mearurements.

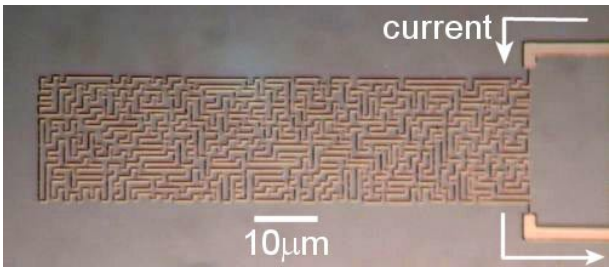

Figure 2.7: Optical micrograph of a NbTi random meander coil

We have made some microscopic wires and meander coils of NbTi using e-beam lithography and co-sputtering technique similar to those mentioned in the last section, and measured the critical current. However the measured critical current remained far less than the expected value as far as we did. The large critical current probably require a fine tuning of the composition of the film and an optimized condition of evaporation.

2.2 Sample preparation and measurement setup

Sample Preparation The 2DES used in the present study are GaAs/GaAlAs single heterojunctions grown with molecular beam epitaxy (MBE). We have used two different 2DES wafers, which are referred to as VG173, VG27 and VG76. The specific parameters that characterize each 2DES wafer are shown in Table 2.1. First, the 2DES wafer is patterned

Table 2.1: 2DES wafers used in this study. Carrier density n_e and mobility μ are often subject to change upon fabrication process.

wafer number	carrier density n_e	mobility μ	depth of 2DES
VG173	2.5×10^{15} m^{-2}	156 m^2/Vs	90 nm
VG27	1.8×10^{15} m^{-2}	40 m^2/Vs	90 nm
VG76	2.1×10^{15} m^{-2}	138 m^2/Vs	274 nm

into a Hall bar-shaped mesa by means of photolithography and wet etching. Ohmic contact electrodes for transport measurements are created with another photolithographic process followed by evaporation of nickel and gold-germanium (AuGe) alloy and annealing at 430°C. Next, a thin, uniform gate electrode of gold covering the Hall bar is fabricated by standard electron-beam lithography, evaporation, and lift-off. The typical thickness of the gate electrode is 20 nm. Finally the magnetic material that produces the MMF is patterned with another e-beam lithography, evaporation, and lift-off process.

6T–1T cross coil superconducting magnet Measurements of magnetotransport were carried out in a cross-coil superconducting magnet system which consists of a 6T split coil and a 1T homemade solenoid (Fig.2.9 left). Samples were mounted on the stage of the rotating stage of the sample holder sketched in Fig.2.9 right. For most measurements in this study, the sample was aligned horizontally so that the 6T split coil serves as the magnet to impose the in-plane field $B_\parallel$, and the 1T solenoid, the perpendicular field $B_\perp$. With the stage rotation, the sample can be aligned to the split magnet within 0.5 degree. The small misalignment can be further compensated with the vertical solenoid, reducing the effective misalignment to 0.01 degree. The azimuthal angle ϕ between the in-plane field $B_\parallel$ and the Hall bar was varied by turning the sample holder about its vertical axis.

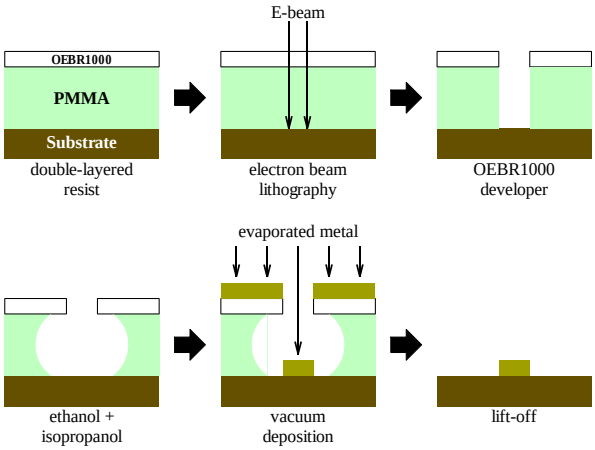

Figure 2.8: Schematic of electron beam lithography and lift-off process. Bi-layer resist is used to make an undercut structure and ease the lift-off.

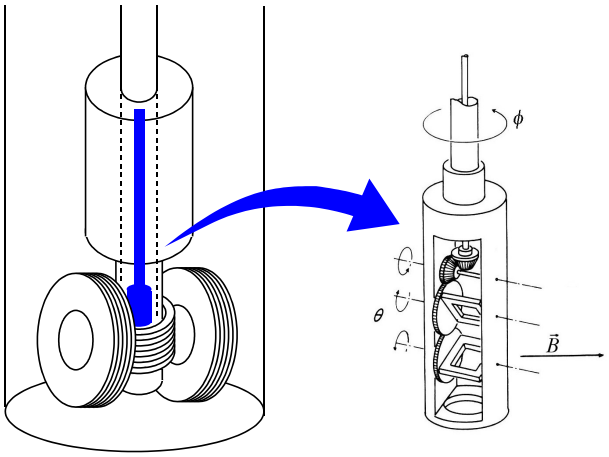

Figure 2.9: Schematic illustration of 6T-1T cross coil superconducting magnet (left) and the sample holder (right).

Transport properties of the 2DES were measured using a standard low-frequency ac technique.

2.3 Profiles of the RMF Samples

In this section, the profiles of the lithographic pattern and the expected magnetic field of the RMF samples that appear in Chap.3 are described. Electronic and geometric properties of each sample follow in Sec.2.3.2.

2.3.1 Lithographic pattern and magnetic field

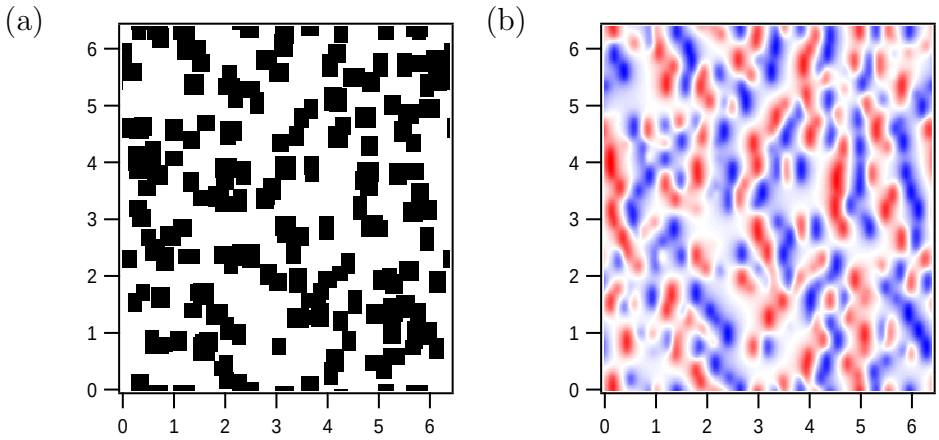

Figure 2.10: (a) lihtographic pattern and (b) expected magnetic field profile of the RMF sample V2717. The unit of the scales of the axes are micron. Red and blue areas in (b) correspond to positive and negative field, respectively.

Fig.2.10 shows the lihtographic pattern and the expected magnetic field profile of the RMF sample V2717. The lithographic pattern consists of rectangular dots randomly displaced within 0.75 μm from square lattice sites with the lattice constant $\bar{a} = 0.5$ μm. Size of each dot is varied randomly within a certain range, 0.35 ± 0.1 μm for this particular sample. Parameters for other samples are summarized in Sec.2.3.2.

The characteristic length scale, or the correlation length ξ_B of the RMF is taken equal to the lattice constant $\bar{a}$ of the underlying lattice. The amplitude $|\delta B|$ of the RMF is determined as $\sqrt{2}$ times the r.m.s. value $\sqrt{\langle \delta B(\boldsymbol{r})^2 \rangle}$ of the magnetic field profile calculated as follows.

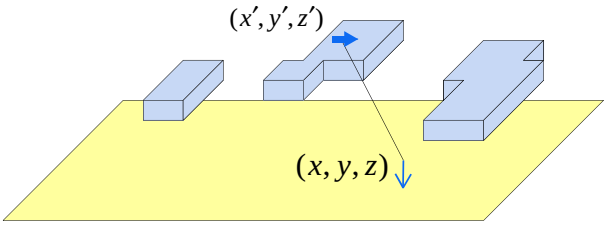

Figure 2.11: The local magnetic field at the 2DES is calculated by integrating the contribution from the magnetic layer.

The lithographic pattern, thickness of the magnetic layer, and the distance of the 2DES plane are taken into account. If the patterned magnetic layer is magnetized uniformly at $\boldsymbol{m}$, the z-component of the magnetic field at $(\boldsymbol{r}, z) = (x, y, z)$ is the sum of the contribution from the whole layer:

$$\boldsymbol{B}(x,y,z) = \int_{\text{pattern}} dx'dy' \int_{\text{thickness}} dz' \frac{1}{4\pi} \left\{ -\frac{\boldsymbol{m}}{R^3} + 3\frac{(\boldsymbol{m}\cdot\boldsymbol{R})\boldsymbol{R}}{R^5} \right\}, \tag{2.3}$$

where $\boldsymbol{R} = (x-x', y-y', z-z')$ and $R = |\boldsymbol{R}|$. For the evaluation of the RMF amplitude $|\delta B|$, the patterned magnetic layer is assumed to be magnetized along the x-axis and the z-compoment of the field at the position of the 2DES is used.

The value of the magnetization are taken 1803 mT for cobalt, 946 mT for NiFe, 461 mT and 625 mT for the two DyCu sample, which are estimated from SQUID measurement. The estimated $|\delta B|$ are just a rough estimate due to the possible errors in the values of the magnetization and the discrepancy of the actual pattern of the magnetic film from the lithographical pattern.

2.3.2 Description of the samples

This section summarizes the electronic and geometrical parameters of the samples presented in this thesis. The correlation length ξ_B and the amplitude $|\delta B|$ characterize the RMF. The carrier density n_e and the mobility μ when the RMF is off characterize the 2DES at the gate voltage applied in the experiment. The items in the geometry are orderd from the top layer of the sample specimen to the 2DES wafer. T, W, and L stand for thickness, width, and length, respectively. $\bar{a}$ is the average spacing between the magnetic dots.

V17303 (from wafer VG173)

$\xi_B = 1\mu$m, $|\delta B| = 37$ mT
$n_e = 2.11\times10^{15}$ m^{-2}, $\mu = 153$ m^2/Vs ($V_g = 0$ mV)
Geometry

DyCu islands	T 185 nm	0.325 μm$\times$ 0.8 μm, $\bar{a} = 1$ μm
Au gate	T 18 nm	
2DES Hall bar	Depth 90 nm	W 20 μm$\times$ L 60 μm

V2717 (from wafer VG27)

$\xi_B = 0.5\mu$m, $|\delta B| = 86$ mT
$n_e = 1.833\times10^{15}$ m^{-2}, $\mu = 39.8$ m^2/Vs ($V_g = 0$ mV)
$n_e = 3.30\times10^{15}$ m^{-2}, $\mu = 47.4$ m^2/Vs ($V_g = +200$ mV)
Geometry

Co islands	T 110 nm	0.35 μm$\times$ 0.35 μm, $\bar{a} = 0.5$ μm
Au gate	T 20 nm	
2DES Hall bar	Depth 90 nm	W 29 μm$\times$ L 130 μm

V2707 (from wafer VG27)

$\xi_B = 1\mu$m, $|\delta B| = 88$ mT
$n_e = 1.991\times10^{15}$ m^{-2}, $\mu = 32.2$ m^2/Vs ($V_g = +150$ mV)
Geometry

Co islands	T 110 nm	0.7 μm$\times$ 0.7 μm, $\bar{a} = 1$ μm
Au gate	T 18 nm	
2DES Hall bar	Depth 90 nm	W 29 μm$\times$ L 130 μm

V2710 (from wafer VG27)

$\xi_B = 1\mu$m, $|\delta B| = 50$ mT
$n_e = 1.956\times10^{15}$ m^{-2}, $\mu = 34.3$ m^2/Vs ($V_g = +700$ mV)
Geometry

Co islands	T 54 nm	0.7 μm$\times$ 0.7 μm, $\bar{a} = 1$ μm
Au gate	T 18 nm	
2DES Hall bar	Depth 90 nm	W 29 μm$\times$ L 130 μm

V2709 (from wafer VG27)

$\xi_B = 1\mu$m, $|\delta B| = 27$ mT
$n_e = 1.887\times10^{15}$ m^{-2}, $\mu = 37.2$ m^2/Vs ($V_\mathrm{g} = +300$ mV)
Geometry

Co islands	T 27 nm	0.7 μm$\times$ 0.7 μm, $\bar{a} = 1$ μm
Au gate	T 18 nm	
2DES Hall bar	Depth 90 nm	W 29 μm$\times$ L 130 μm

V2703 (from wafer VG27)

$\xi_B = 0.5\mu$m, $|\delta B| = 36$ mT
$n_e = 2.37\times10^{15}$ m^{-2}, $\mu = 42.6$ m^2/Vs ($V_\mathrm{g} = 0$ mV)
Geometry

DyCu islands	T 185 nm	0.25 μm$\times$ 0.25 μm, $\bar{a} = 0.5$ μm
Au gate	T 18 nm	
2DES Hall bar	Depth 90 nm	W 20 μm$\times$ L 60 μm

V7605 (from wafer VG76)

$\xi_B = 1\mu$m, $|\delta B| = 25$ mT
$n_e = 2.56\times10^{15}$ m^{-2}, $\mu = 200$ m^2/Vs ($V_\mathrm{g} = +300$ mV)
Geometry

Au gate	T 60 nm	
NiFe islands	T 225 nm	0.5 μm$\times$ 0.5 μm, $\bar{a} = 1$ μm
2DES Hall bar	Depth 274 nm	W 33 μm$\times$ L 100 μm

Chapter 3

Experimental Results and Discussion

We first discuss the experiments on 2D random magnetic field (RMF). The samples were prepared by depositing DyCu alloy or cobalt on the 2DES Hall bar in a random pattern as described in Sec.2.3.

We should note that the random magnetic field component $\delta B(\boldsymbol{r})$, which is controlled via the in-plane external field $B_{\|}$, is dependent on the azimuthal angle of $B_{\|}$ in the xy-plane, and is not isotropic because each magnetic particle with an in-plane magnetic moment imposes on the 2DES a pair of positive and negative field modulation around itself, aligned with others. However the realized MMF is considered to have the feature of the RMF in that it does not have a particular modulation wave vector by which it is characterized. For the experimental results presented in this section, the in-plane external field $B_{\|}$ is oriented parallel to the current $\boldsymbol{J}$.

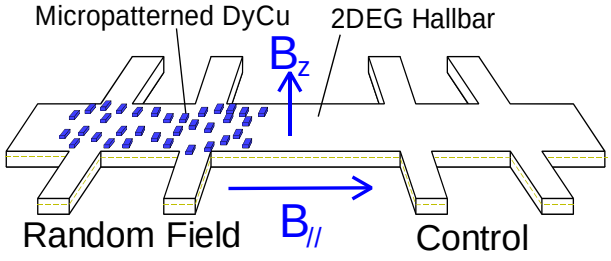

Figure 3.1: Schematic of patterned magnet for random magnetic field (RMF).

3.1 Resistance increase due to zero-mean RMF

Let us start with a RMF with zero mean, *i.e.* $\delta B \neq 0$ with $\bar{B} = 0$. As discussed in Chap.2, this configuration is realized by applying the external magnetic field $B_{\parallel}$ parallel to the 2DES plane. 2DES with random DyCu islands is used for this purpose in order to study the dependence of the resistance on the amplitude of the RMF, which will be denoted by $|\delta B|$. It is for the DyCu with no hysteresis loop that the magnetization M, and therefore also $|\delta B|$, can be expressed as a single valued function of $B_{\parallel}$. Figure 3.2 (a) shows the magnetization curve of the uniform DyCu film deposited at the same time as that on the measured 2DES Hall bar. The magnetization grows rapidly at low field and reaches close to its saturation value at 2∼3 T.

Figure 3.2 (b) shows the resistivity of the 2DES with the randomly patterned DyCu islands, as a function of the in-plane field, together with the data for a control sample without the DyCu. The resistance of the former shows a considerably larger increase than the control sample as the RMF is turned on. This increase can be attributed to the increased scattering of the electrons by the RMF. There is also a small increase in the resistance of the control sample at higher fields. This is probably due to the modification of the wave function in the direction perpendicular to the 2D plane caused by the in-plane field. Although dependences of its magnitude on carrier density, mobility, or azimuthal direction of the in-plane field, is unknown, it is negligibly small in the low-field region below 3 T, where the amplitude of the RMF grows rapidly.

Figure 3.3 (a) shows the results of similar measurements with different gate voltages $V_{\rm g}$ on the uniform gate under the patterned DyCu on the 2DES Hall bar. To examine the RMF-amplitude dependence of the 2DES resistivity, the resistance increase is replotted as a function of the magnetization of the DyCu (Fig.3.3(b)). In order to compare the results for different values of $V_{\rm g}$, the relative change $\Delta\rho/\rho^0$ is plotted. Though $\Delta\rho$ appear to be larger for larger negative $V_{\rm g}$, those rescaled with ρ^0 fall under the same scale. Setting aside the high-field region where magnetoresistance due to $B_{\parallel}$ itself becomes distinct, $\Delta\rho/\rho^0$ is proportional to M^2 for all gate voltages. We did not find singular behavior that may reflect the change in the symmetry class with the introduction of the RMF. This result corroborates the simple expectation that the additional scattering rate caused by the RMF is proportional to the square of the RMF amplitude.

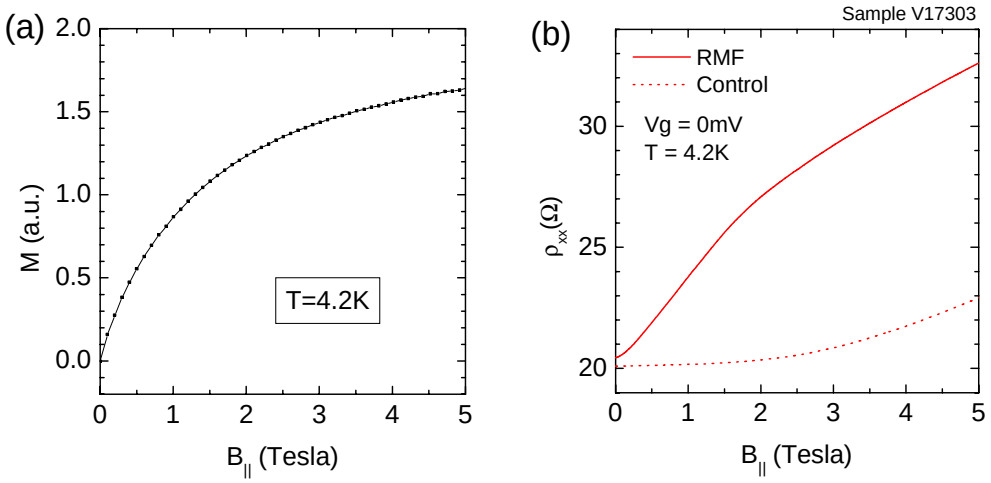

Figure 3.2: (a) Magnetization of the DyCu film (b) Resistance of the 2DES with and without the ramdomly patterned DyCu, as functions of the in-plane external field.

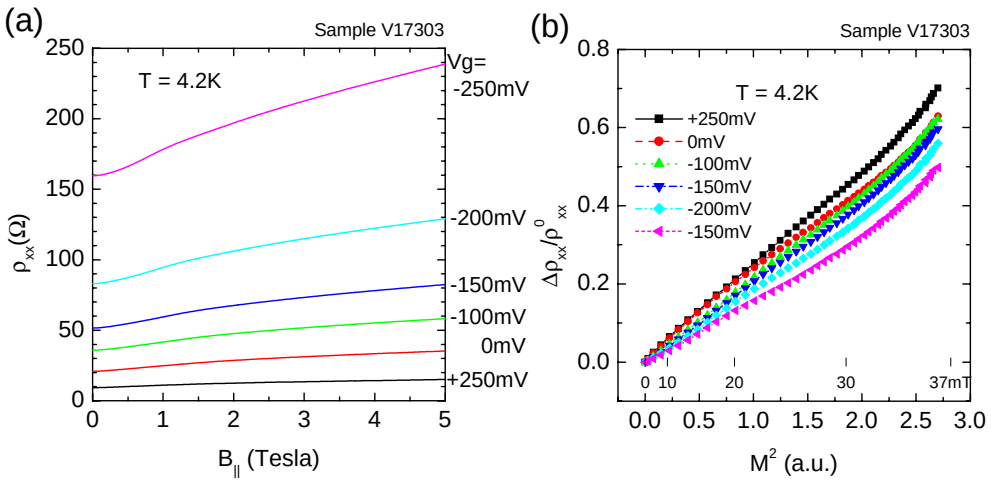

Figure 3.3: (a) Resistivity of the 2DES with random DyCu for different gate voltages. (b) Relative change in the resistivity plotted against the square of the magnetization of DyCu.

3.2 Magnetoresistance in RMF

Fixing the random field component $\delta B(\boldsymbol{r})$ with the strong in-plane external field $B_{\|}$, we can independently apply a uniform perpendicular field $\bar{B}$ with the inner solenoid. Figure 3.4 shows the resistivity of the 2DES as a function of $\bar{B}$ for five different temperatures. The magnetoresistance in the presence of RMF has some distinctive features. It draws a large positive curve, with a shoulder-like structure indicated by the arrows, until the onset of Shubnikov-de Haas (SdH) oscillation, and reaches almost twice the value at $\bar{B} = 0$. It has a smaller downward cusp structure indicated by the circle near $\bar{B} = 0$, which is commonly observed in different samples. The low-field structure have only small temperature dependence while the SdH oscillation have a strong temperature dependence in this temperature range. These features of the magnetoresistance are reminiscent of those in a plain 2DEG around the half-filled Landau level state. The magnetoresistance curves in Figures 3.4 and 1.9 (page 14) actually look very similar to each other, except for the scales of the axes. The fact that the magnetoresistance of the two systems look similar provides a strong support to the mapping between the two. To further discuss the relevance of the RMF system to the CF system, we should consider the nature of the structures in these positive magnetoresistance.

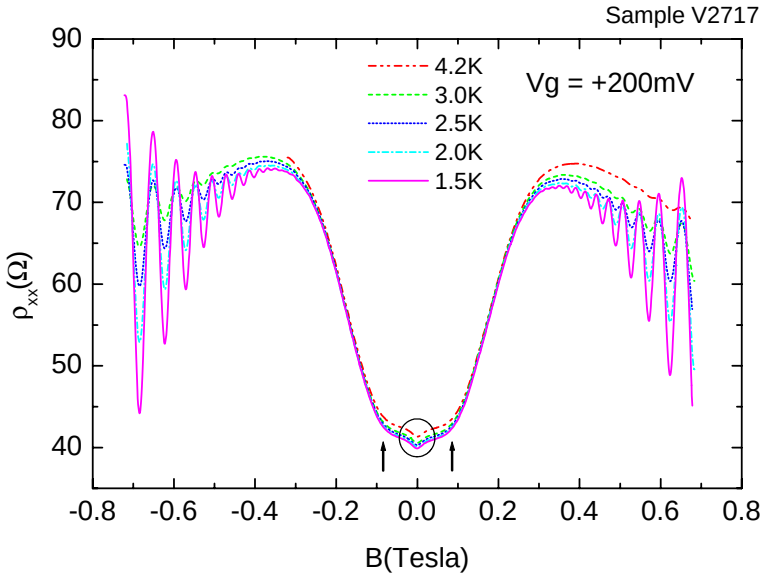

Figure 3.4: Magnetoresistance with respect to the uniform field component, at different temperatures. The circle and the arrows indicate the "center cusp" and the "broad shoulders", respectively.

3.2.1 Structures in the magnetoresistance

The robustness to the temperature compared to the SdH oscillation suggests that the structures in the magnetoresistance are of semiclassical nature. Hedegård *et al.*'s semiclassical theory [45] introduced in Sec.1.4.3 seems to cover the situation realized in our experiment. They show the calculated magnetoresistance in fixed RMF for some representative values of n_e, δB, l, and ξ_B. The behavior of the magnetoresistance curve depends largely on the ratio l/ξ_B of the mean free path to the RMF correlation length. The result for $l/\xi_B = 5$ and 10, the values close to l/ξ_B in our systems, also show positive magnetoresistance with a peculiar structure at low-field (Fig.1.11). Its magnitude and range is smaller than our data probably because the modulation amplitude is much weaker. However we cannot determine if this explains our experimental data since they did not address the physical picture of these behavior of the magnetoresistance. Here, let us consider the nature of the structures seen in our experiment by analogy to those in 1D periodic systems.

The downward cusp structure at $\bar{B} = 0$ is also observed in 1D periodic systems, and considered to be associated to the snake orbits (Fig.3.5 (a)). We can imagine similar orbits, also for RMF, that meander between positive and negative regions of local field $B(\boldsymbol{r})$ and drift along $B(\boldsymbol{r}) = 0$ contour as in Fig.3.5 (b). Mirlin *et al.* [43] argue that such orbits play an essential role in the low-field transport in the presence of RMF, though they assume the limit of extremely long mean free path.

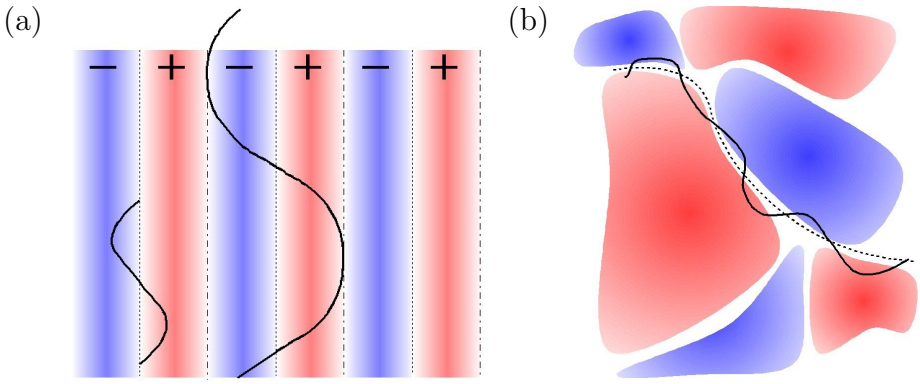

Figure 3.5: Snake orbits for (a) 1D periodic and (b) random magnetic fields.

At the intermediate field region, a 1D periodic system shows the Weiss oscillation, an oscillatory magnetoresistance from commensurability between the modulation period a and the cyclotron diameter $2R_c$. In the

case of RMF, we do not see such oscillation because there is no particular modulation period. Instead, there is a characteristic length scale ξ_B of the RMF correlation that correspond to a for a periodic system. The shoulder-like structure is possibly related to the crossover of the cyclotron motion with the RMF correlation length ξ_B.

The following magnetoresistance data taken for various RMF samples are compatible with these pictures.

Dependence on gate voltage Figure 3.6 shows the results of similar measurements with different gate voltages $V_{\rm g}$. Each resistance curve is rescaled with its $\bar{B} = 0$ value for comparison. With more positive $V_{\rm g}$, the structures in the magnetoresistance curve mentioned earlier become clearer.

Particularty the center cusp gets pronounced for $V_{\rm g} \geq +100$mV. Since the gate voltage changes both the carrier density n_e and the mobility μ of the 2DES, it is difficult to single out the effect of either one. Instead, the mean free path $l = v_{\rm F}\tau = (\hbar/e)\sqrt{2\pi n_e}\,\mu$ would be a good measure of the transport property. The electron mean free path obtained for the above data is $l \approx 2$ μm at $V_{\rm g} = 0$ mV, $l \approx 4$ μm at $V_{\rm g} = +180$ mV, while the RMF correlation length is $\xi_B \approx 0.5$ μm for this sample. It seems that the center cusp requires an electron to travel several times the correlation length before it is scattered away. In the context of snake orbit, the center cusp requires the formation of well-defined snake orbits that experience more than few sign alternation in the local field $B(\boldsymbol{r})$.

Dependence on RMF amplitude and correlation length We have done measurements on many samples with different patterns and thickness of magnetic films on the 2DES Hall bar. These difference can be described with two parameters, $|\delta B|$ and ξ_B, that characterise the RMF. The condition of the 2DES also differed sample by sample and this made the systematic study difficult, but we can still grasp some tendency that support our semi-classical picture in the magnetoresistance curves from the available data.

Figure 3.7 shows the magnetoresistance of three RMF samples with the same lithographic pattern but with different thickness of the magnetic layer. The magnetoresistance of a 2DES without magnetic film is also shown for comparison. The gate voltage was adjusted before this measurement so that the resistivity of the four samples are about the same value when the RMF is off. The carrier densities and the mobilities take slightly different values but are still close to each other. The resistivity at $\bar{B} = 0$ in the figure, with the RMF turned on, is larger for the sample with larger RMF amplitude.

We can see from the figure that the positive magnetoresistance with

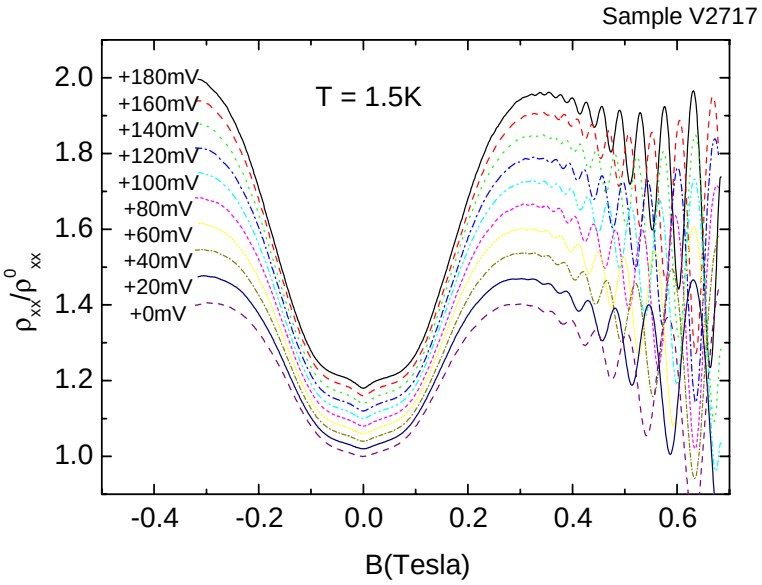

Figure 3.6: Magnetoresistance with respect to $\bar{B}$ for different gate voltages. Traces are vertically shifted for clarity.

respect to $\bar{B}$ is also larger for larger $|\delta B|$. In Fig.3.7(b), the trace near $\bar{B}$ is enlarged. Here we find that the trace for $|\delta B| = 27$mT shows a signature of the center cusp and the broad shoulders while that for $|\delta B| = 88$mT is rather featureless in spite of the larger $|\delta B|$. This is because the RMF itself diminishes the electron mean free path and smears out the fine structures in the magnetoresistance.

Figure 3.8 shows the magnetoresistance of another four samples. The carrier density, mobility, RMF amplitude and correlation length take various values. This comes out as the variety in the vertical scale but let us focus on the horizontal ($\bar{B}$-) axis here. We can find the following features.

1. The broad shoulder appears at $\bar{B} \approx 0.05$T for samples with $\xi_B = 1\mu$m, and at $\bar{B} \approx 0.1$T for samples with $\xi_B = 0.5\mu$m. This suggests that this broad structure is related to the crossover of the cyclotron radius $R_c = k_F l_B^2$ with the characteristic length ξ_B of the RMF. Cyclotron radius is $R_c \approx 1.5\mu$m and 0.7μm at $\bar{B} = 0.05$T and 0.1T, respectively.

2. The center cusp appears regardless of the modulation amplitude if the electron mean free path is sufficiently long. Its width is approximately $|\delta B|$. Snake orbits that meander along the $B(\boldsymbol{r}) = 0$ contour, where $B(\boldsymbol{r}) = \bar{B} + \delta B(\boldsymbol{r})$, require the modulation amplitude $|\delta B|$ to be larger than the uniform background field $\bar{B}$. The relation of the RMF am-

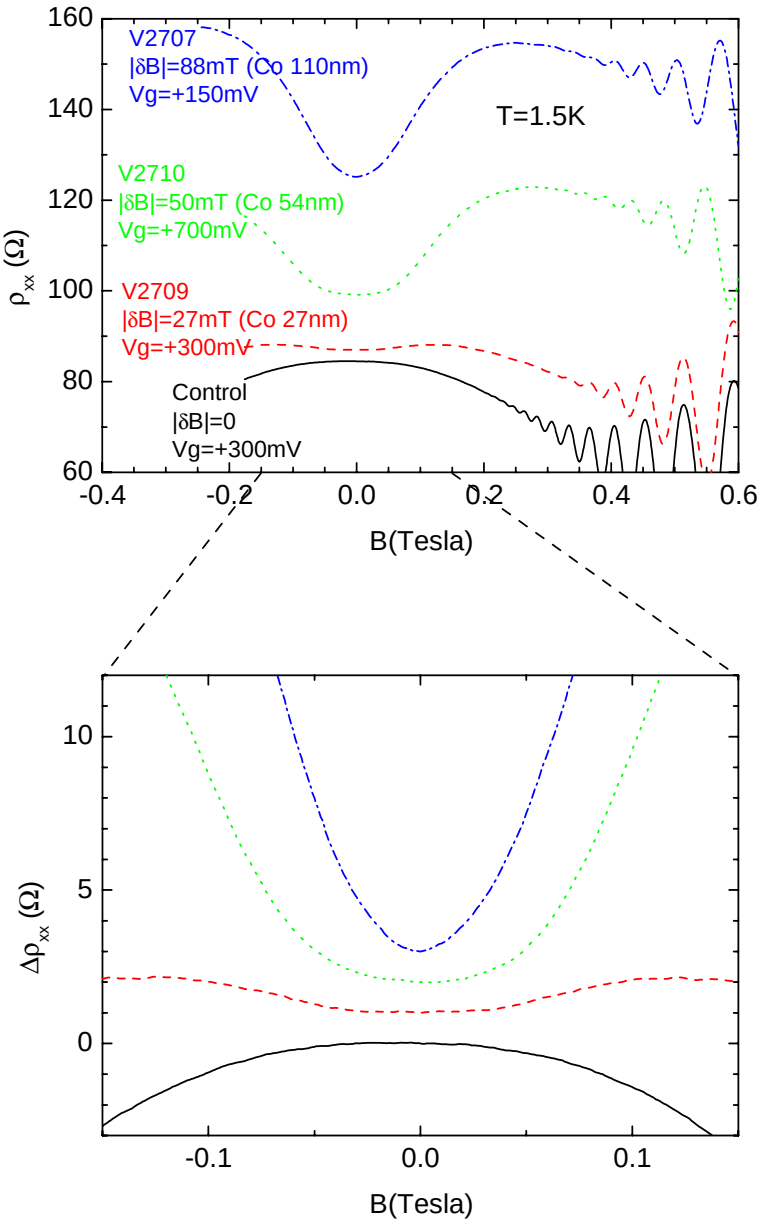

Figure 3.7: Magnetoresistance of RMF samples with different RMF amplitudes and a 2DES without RMF. (a) is the actual resistivity and (b) shows the change from its $\bar{B} = 0$ value with vertical shifts.

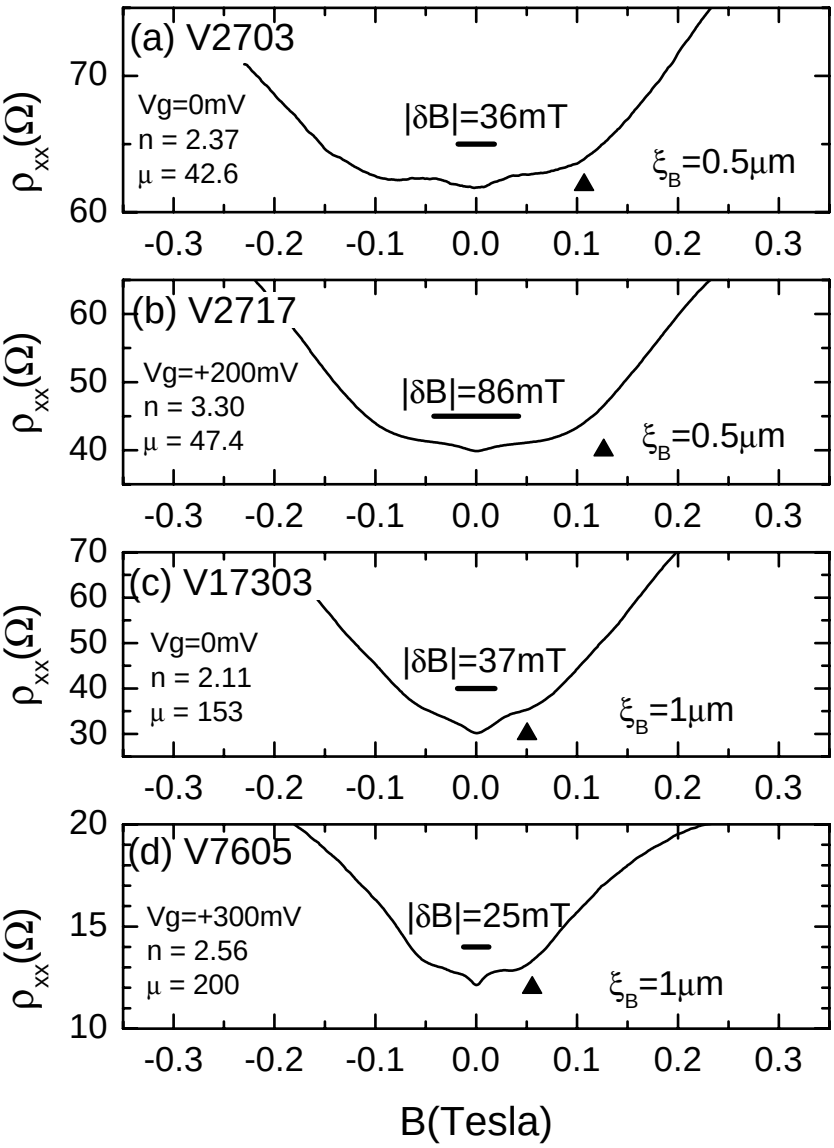

Figure 3.8: Magnetoresistance of various RMF samples. The filled triangle indicate the magnetic field value where $R_c = 1.5\xi_B$. The horizontal bars correspond to $|\delta B|$. The units for the carrier density n and the moblity μ are $10^{15}\mathrm{m}^2$ and m^2/Vs, respectively.

plitude with the width of the conter cusp gives further support to the relevance of snake orbit to the center cusp.

Table 3.1: RMF correlation length ξ_B and cyclotron radius R_c at the broad shoulder.

Sample	ξ_B	$\bar{B}$ at shoulder	R_c at shoulder
RMF	1μm	0.06T	1.5μm
RMF	0.5μm	0.12T	0.7μm
CF [37]	100nm	0.6T	160nm

Comparison with the composite fermion system Assuming that the magnetoresistnace curve around the half-filled Landau level state in Fig.1.9 is of the same nature with our data, properties of the effective RMF in CF system can be deduced. The magnetoresistance curve in Jiang *et al.*'s data [37] is centered at $B_{1/2} \approx 13.4$ T, with the center cusp between $\approx B_{1/2} \pm 0.2$ T and the broad shoulder at $\approx B_{1/2} \pm 0.6$ T. The width of the center cusp gives the amplitude $|\delta B| \approx 0.2$ T of the effective RMF, which correspond to the amplitude of local charge density fluctuation

$$\frac{\delta n_e(\boldsymbol{r})}{n_e} \approx \frac{|\delta B|}{B_{1/2}} \approx \frac{0.2\ \mathrm{T}}{13.4\ \mathrm{T}} \approx 1.5\%. \tag{3.1}$$

The CF cyclotron radius at the broad shoulder

$$R_c^{\mathrm{CF}} = k_{\mathrm{F}}^{\mathrm{CF}} l_B^2 = \frac{\hbar}{e} \times \sqrt{4\pi n_e} \times \frac{1}{0.6\ \mathrm{T}} \approx 160\mathrm{nm} \tag{3.2}$$

gives the measure of the RMF correlation length ξ_B. Here we used the carrier density $n_e = 1.7{\times}10^{15}$ m^{-2} taken from Ref. [37]. This agrees with the argument that the RMF correlation length for the CF systems is about 100 nm because the density fluctuation is created by ionized impurities at the doping layer typically located 100 nm away from the 2DES.

3.2.2 Shubnikov-de Haas oscillation

The amplitude $\Delta\rho_{\mathrm{SdH}}$ of the Shubnikov-de Haas (SdH) oscillation, normalized to classical resistivity ρ_0 is well described by the formula [52, 53]

$$\frac{\Delta\rho_{\mathrm{SdH}}}{\rho_0} = \frac{A_T}{\sinh A_T} \exp\left(-\frac{\pi}{\omega_c \tau_{\mathrm{tot}}}\right). \tag{3.3}$$

Here, $A_T = 2\pi^2 k_B T/\hbar\omega_c$ accounts for thermal smearing, $\omega_c = eB/m^*$ is the cyclotron frequency for effective mass m^*, and $1/\tau_{tot}$ is the total scattering rate. This expression is often used to deduce m^* and τ_{tot} from the temperature- and magnetic field dependence of the SdH amplitude, which is experimentally available.

Du *et al.* adopted this formula to analyze the FQH oscillations around $\nu = 1/2$ and determined the effective mass m^*_{CF} of the composite fermion to be about an order of magnitude larger than the band mass $m^* \approx 0.067m_e$ of GaAs [38]. They also argued that m^*_{CF} is dependent on magnetic field and diverges toward the exact half filling at $B = B_{1/2}$ [39]. Mancoff *et al.* [49] performed the analysis with the SdH oscillation in their 2DES sample with RMF produced with rough-surface ferromagnet. They did not find any significant change in the electron effective mass and concluded that the physics around $\nu = 1/2$ may differ substantially from simple 2D transport in RMF. The samples used by Mancoff *et al.*, however, were such that the electron mean free path was shorter than the characteristic length scale of the RMF. In other words, the experimental situation in their samples should be viewed as macroscopically inhomogeneous magnetic field rather than true RMF.

It is therefore worthwhile to carry out a similar analysis on the data from our samples which differ from those of Mancoff *et al.* in that the electron mean free path is longer than the characteristic length scale of the RMF. Figure 3.9 shows an example of the analysis procedure. We start from the magnetoresistance described in Sec.3.2, measured at different temperatures (Fig.3.9 (a)). The oscillating part is extracted by subtracting the smooth background (Fig.3.9 (b)), and its extrema are taken as the SdH amplitudes $\Delta\rho_{SdH}$. The subtracted background is also used as the classical resistivity ρ_0 at each magnetic field. Figure 3.9 (c) shows the temperature dependence of $|\Delta\rho_{SdH}|/\rho_0$ for six different SdH extrema. Fitting to the T-dependent part $A_T/\sinh A_T$ in the formula (3.3) yields the effective mass m^* for each peak or dip. For this particular set of data, it is found to be $m^*/m_e = 0.075 \pm 0.002$. Figure 3.9 (d) is the so-called Dingle plot, which is a plot of

$$S = \ln\left[\frac{\Delta\rho_{SdH}}{4\rho_0} \cdot \frac{\sinh A_T}{A_T}\right] \tag{3.4}$$

against the inverse magnetic field $\bar{B}^{-1}$. Data from RMF sample, as well as the data from control sample on the same specimen, are shown using the effective mass obtained in the previous plot. The Dingle plot should fall on a single straight line with the slope corresponding to the total scattering rate $1/\tau_{tot}$, if the SdH amplitude is in accordance with (3.3). Both data from RMF and control samples are well fitted by linear function, except for

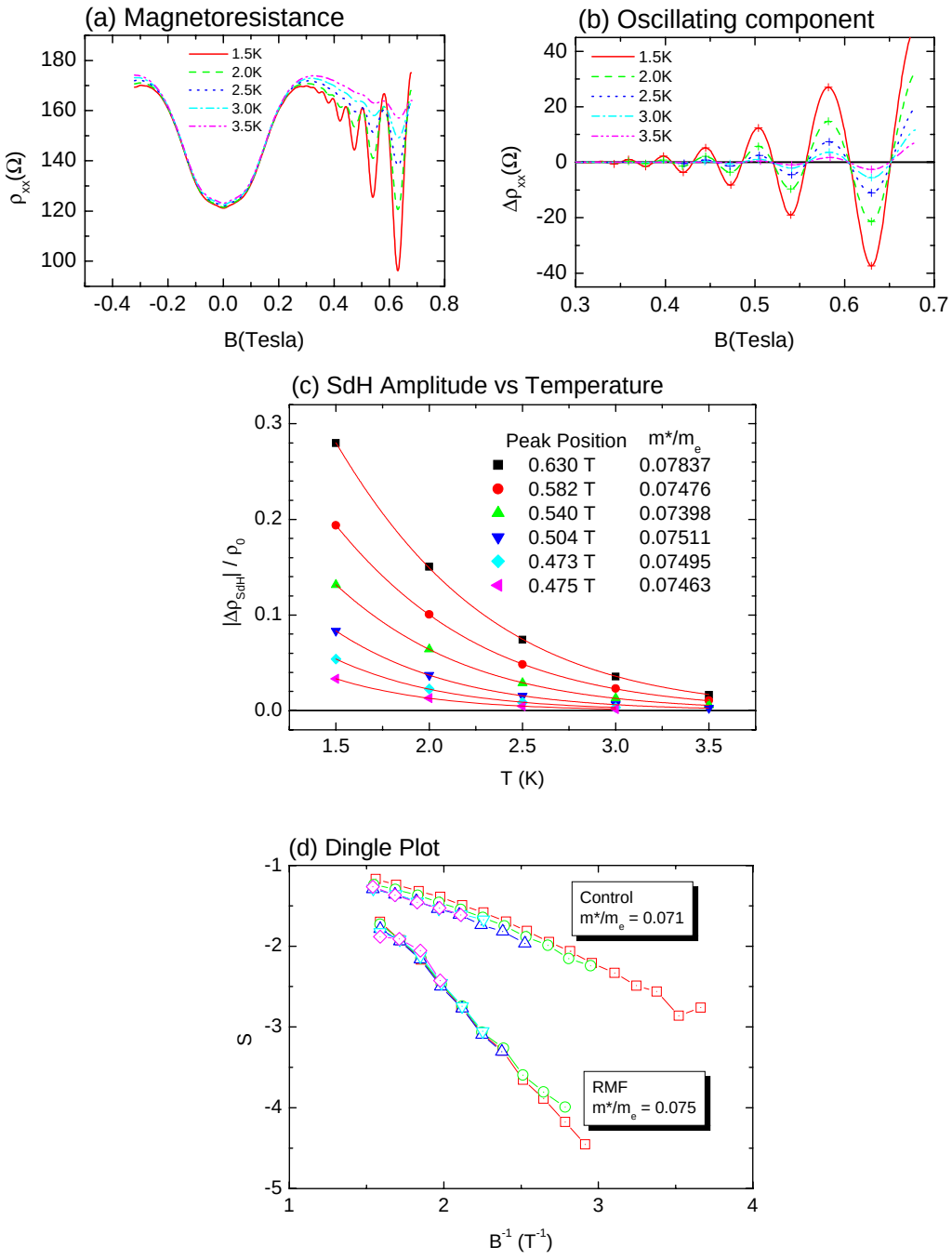

Figure 3.9: (a) Magnetoresistance with respect to five different temperatures. (b) Oscillating component extracted from (a). (c) Rescaled amplitudes of the SdH extrema plotted against temperature. (d) Dingle plot: $S = \ln[\frac{|\Delta\rho_{\mathrm{SdH}}|}{4\rho_0}\frac{\sinh A_T}{A_T}]$ vs. $\bar{B}^{-1}$. Data shown in this figure is taken for the sample V2717 with $V_{\mathrm{g}} = 0$.

the high-field region where the SdH oscillation crosses over to the QHE and deviates from (3.3).

Table 3.2 summarises the effective mass m^* and total scattering time $\tau_{\rm tot}$ determined from the SdH analysis together with the momentum relaxation rate τ determined from the resistivity $\rho_0 = m^*/n_e e^2\tau$ at $\bar{B} = 0$. Data from Ref. [49] are also shown.

Table 3.2: Effective mass m^* and total scattering time $\tau_{\rm tot}$ obtained from the analysis of SdH oscillation together with some relevant parameters.

Sample	$\lvert\delta B\rvert$	ξ_B	m^*/m_e	$\tau_{\rm tot}$	τ
V2709 Control	0	—	0.074	1.84ps	14.2ps
V2709 RMF	27mT	1μm	0.074	0.94ps	13.2ps
V2710 RMF	50mT	1μm	0.074	0.56ps	10.9ps
V2707 RMF	88mT	1μm	0.072	0.50ps	8.5ps
V2717 Control	0	—	0.071	1.53ps	14.2ps
V2717 RMF	86mT	0.5μm	0.074	0.63ps	10.5ps
Mancoff [49] Control	0	—	0.06	0.94ps	38.1ps
Mancoff [49] RMF	100mT	20μm	0.06	0.32ps	3.8ps

The effective mass m^* does not seem to show a significant change in the presence of the RMF. This confirms the argument that the enhancement of CF effective mass cannot be explained by the static RMF as realized in this experiment. It implies that the mass enhancement is rather due to the dynamical field fluctuation that arise from electron correlation.

Presence of RMF significantly reduces the total scattering time $\tau_{\rm tot}$ than the momentum relaxation rate τ. This implies that the RMF introduces many small angle scattering events. Possible reason for the apparently opposite tendency of Mancoff *et al.*'s result to ours is that they have underestimated the momentum relaxation time τ in the presence of RMF because zero-mean RMF could not be realized in their sample.

3.2.3 Effect of randomness on 1D modulation

In Sec.3.2.1, we have discussed the magnetoresistance in RMF by analogy to those in 1D periodic MMF because the physics of 2DES in regular 1D MMF is well established as we have seen in Sec.1.2. In this section, we introduce randomness to the 1D MMF system in order to acquire better understanding on the physics of 2DES in random magnetic field.

The samples used here are 2DES Hall bar with ferromagnetic strips with different degrees of randomness. The lithographical patterns to fabricate these samples consist of lines and spaces, whose widths are varied randomly within the range listed in Fig.3.10. Figure 3.10 also shows the scanning electron micrograph of the four patterns, together with the Fourier spectra of the calculated magnetic field profile.

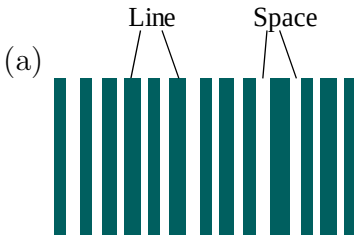

(b)

Sample	line	space
LS04	0.2μm	0.3μm
LS05	0.2±0.05μm	0.3±0.05μm
LS06	0.2±0.1μm	0.3±0.1μm
LS07	0.2±0.2μm	0.3±0.2μm

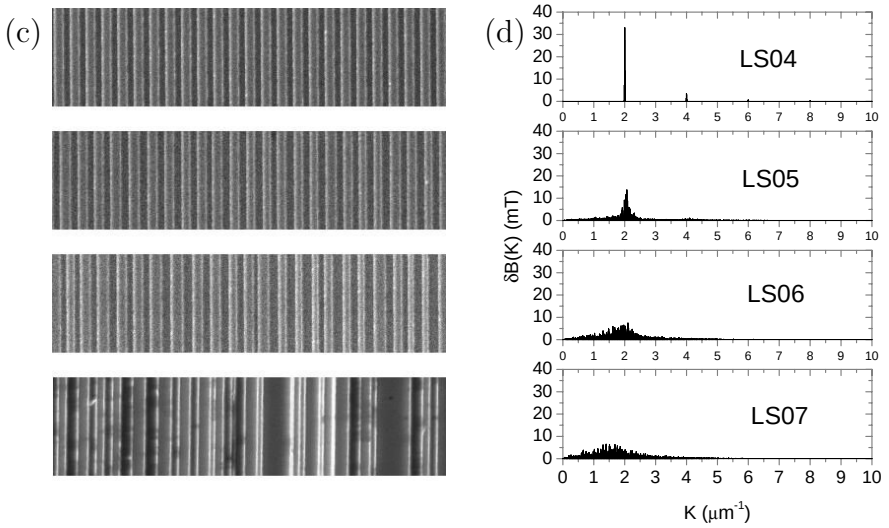

Figure 3.10: (a) Schematic of the lithographical pattern for random 1D MMF. (b) Parameters of the four samples. The lower pattern is more disordered. (c) Scanning electron micrographs of the four samples. (d) Fourier spectrum $\delta B(K)$ of the expected MMF for the four samples.

The measurement of the magnetoresistance is done in the same way as we did in Sec.3.2 for the magnetoresistance of RMF sample. Fig.3.11 shows the magnetoresistance with respect to $\bar{B}$ in fixed modulation $\delta B(\boldsymbol{r})$, for the four samples listed above. The sample LS04 without randomness shows a clear mangetic Weiss oscillation. The vertical lines indicate the expected positions of the resistivity minima (1.16). The positive magnetoresistance, or the downward "center cusp", near $\bar{B} = 0$ with the snake orbit (see Sec.1.2.2) is also observed. For samples LS05, LS06, and LS07

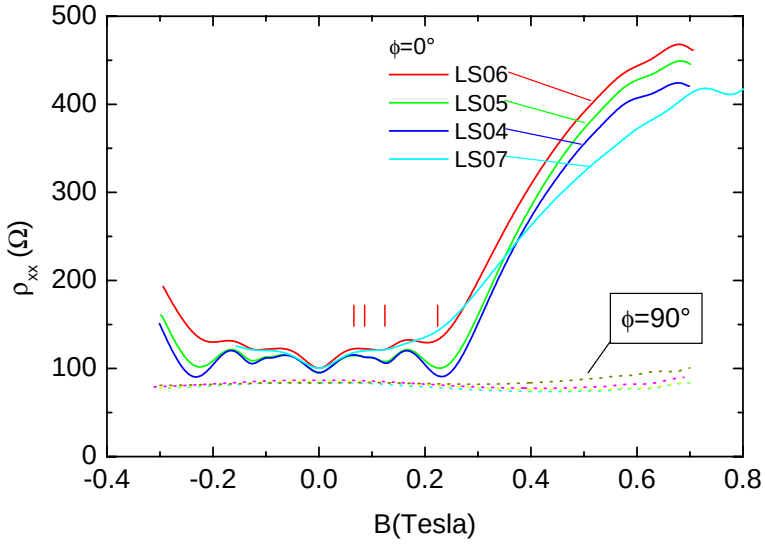

Figure 3.11: Magnetoresistance of the four random 1D MMF samples. Vertical lines indicate the expected dip positions for the regular one, LS04.

with increased randomness, the center cusp persists while the commensurability oscillation becomes weaker and the main resistance minimum at $\bar{B} = 0.22$ T turns into a broad shoulder-like structure similar to that seen in RMF samples. For the sample LS07 with the largest extent of randomness, the overall shape of the magnetoresistance trace resembles that for RMF samples. This implies that for random MMF, its dimensionality does not lead to a qualitative difference in the magnetoresistance of the 2DES. However a thorough understanding on these magnetoresistance needs more investigation from the theoretical side.

3.2.4 Remarks on anisotropy

We have noted at the beginning of the chapter that the RMF realized in our samples have some anisotropy associated with the azimuthal angle of the in-plane field $B_{\|}$. We can actually change the azimuthal angle by turning the sample holder about its vertical axis. Fig.3.12 shows a magnetoresistance for different azimuthal angles, $\phi = 0°$ and $90°$, where ϕ is defined as the angle between $B_{\|}$ and the direction of the current (x-axis). The features of the two data are very similar except that the data for $\phi = 0°$ shows a larger positive magnetoresistance.

The magnetic field profile shown in Fig.2.10 (page 28), which is calculated for $\phi = 0°$, exhibit many pairs of positive and negative field region

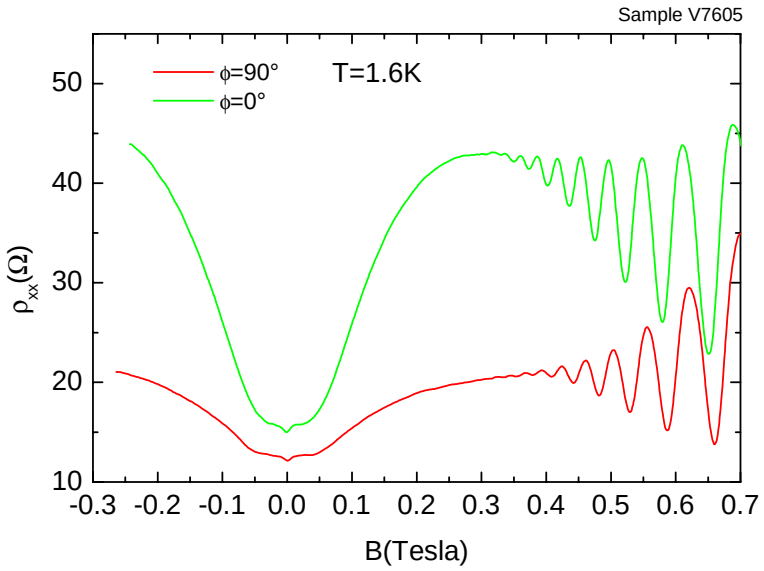

Figure 3.12: Magnetoresistance for $\phi = 0°$ and $\phi = 90°$.

aligned in x-direction. This implies that the RMF in the case of $\phi = 0°$ contains more x-components in its Fourier spectrum. In other words, if the Fourier spectrum of an isotropic RMF is expressed as an circle cloud with the diameter about ξ_B^{-1}, that for the RMF for $\phi = 0°$ is distorted in the x-direction. As the x-component ρ_{xx} of the resistivity is mainly determined from the modulation component in the x-direction, and ρ_{yy} from those in the y-direction, the larger magnitude in the positive magnetoresistance is due to the larger weight in the modulation component parallel to its direction.

On the other hand, the similarity of the two curves implies that the characteristic features in the magnetoresistance curve are quite general among certain class of RMF and that the magnetoresistance for isotropic RMF would show a similar behavior without the difference in magnitude between ρ_{xx} and ρ_{yy}.

3.3 Temperature dependence of the resistivity in zero-mean MMF

Recent experimental and theoretical studies on 1D perodic MMF [20,21] revealed that a 2DES shows a T^2-dependent resistivity component in the presence of such modulation. The occurrence of T^2-dependent resistivity component is explained that the MMF gives rise to umklapp electron-electron

scattering events that change the total momentum and contribute to resistivity. Such mechanism should be at work if the translational symmetry of the system is broken, even if there is no specific modulation wave vector K as in regular MMF.

In order to prove this idea, we have measured the temperature dependence of 2DES in random 1D, regular 2D, and random 2D MMFs.

3.3.1 1D modulation

Figure 3.13(a) shows the temperature dependence of the resistivity of 1D MMF samples LS04∼07, for the maximum modulation (azimuthal angle of the in-plane field set at $\phi = 0°$) and no modulation ($\phi = 90°$). For all samples the resistivity shows a non-linear increase with respect to the temperature T only in the presence of the MMF. Figure 3.13(b) shows the change in resistivity $\Delta\rho = \rho(\phi = 0°) - \rho(\phi = 90°)$ due to the MMF. A fit of the $\Delta\rho$ for $3\mathrm{K} < T < 10\mathrm{K}$ to the form

$$\Delta\rho = AT^2 + BT + C \tag{3.5}$$

gives the coefficients summarized in Table 3.3.

Table 3.3: Temperature dependence coefficient of the resistivity.

Sample	$n_e(10^{15}\mathrm{m}^{-2})$	$\mu(\mathrm{m}^2/\mathrm{Vs})$	$A(\Omega/\mathrm{K}^2)$	$B(\Omega/\mathrm{K})$	$C(\Omega)$
LS04	1.804	43.1	0.071	−0.21	9.64
LS05	1.810	42.3	0.073	−0.19	10.75
LS06	1.810	42.3	0.083	−0.16	14.56
LS07	2.255	35.0	0.034	+0.06	16.26

Excepting the sample LS07, whose carrier density n_e and mobility μ is significantly different from the others, the coefficient A of the T-quadratic term and the constant term C are both larger for larger degree of randomness. Introduction of randomness not only broadens the Fourier spectrum of the MMF, but also shifts its center to the smaller K (longer wavelength) side (Fig.3.10). Since the formula of the resistance increase (1.22) by Sasaki *et al.* indicates that the modulation with longer wavelength contributes more to both A and C terms, the shift in the Fourier spectrum of MMF may be the reason for increased coefficients with randomness. However the validity of Eq.(1.22) for the case of distributed Fourier components of modulation have to be examined.

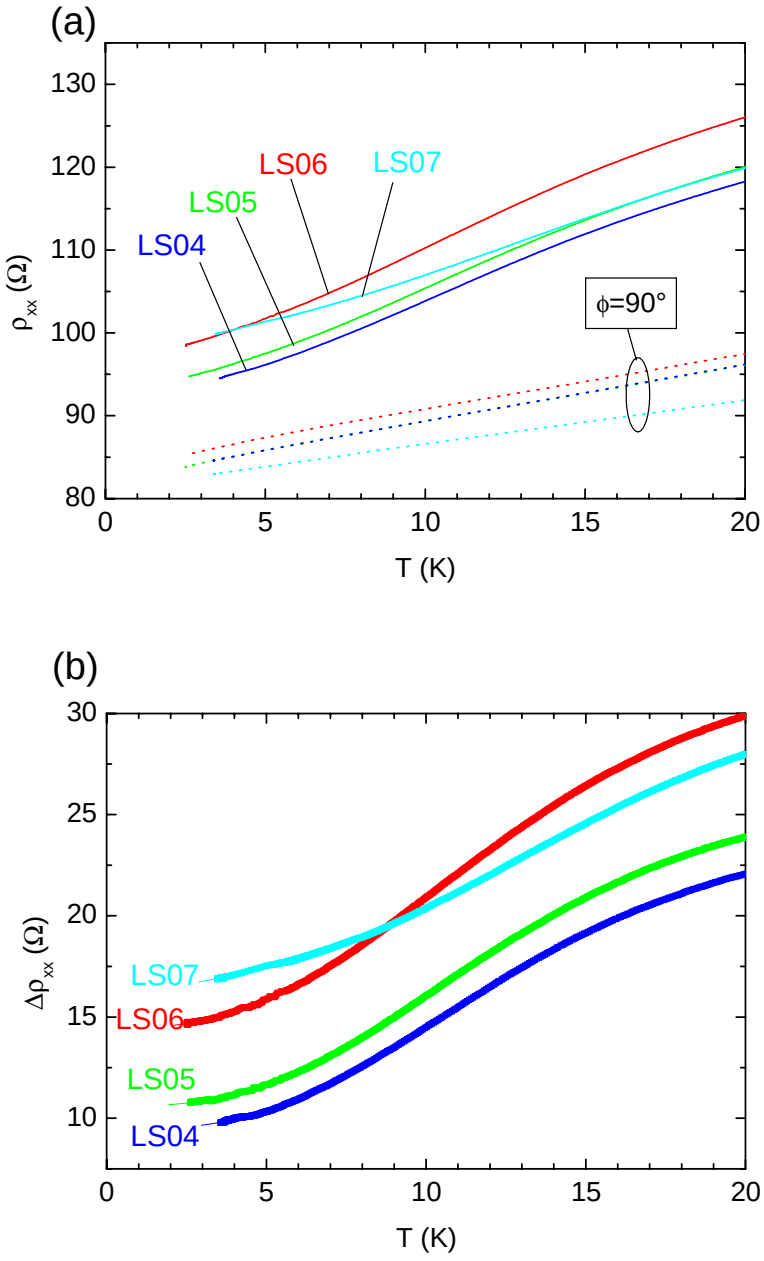

Figure 3.13: (a) Temperature dependence of the resistivity of random 1D MMF samples. The solid lines are for the maximum modulation and the dotted lines indicated by $\phi = 90°$ are for no modulation. (b) Difference in the resistance between the presence and absence of the MMF.

3.3.2 2D modulations

Figure 3.14 shows the temperature dependence of a RMF sample studied in Sec.3.1. Unlike the 1D MMF samples, the resistance appears to be linear in T when the RMF is turned on by the in-plane field. We have also done a similar measurement on a 2DES with regular 2D MMF, which also did not show a T^2-dependent resistivity component.

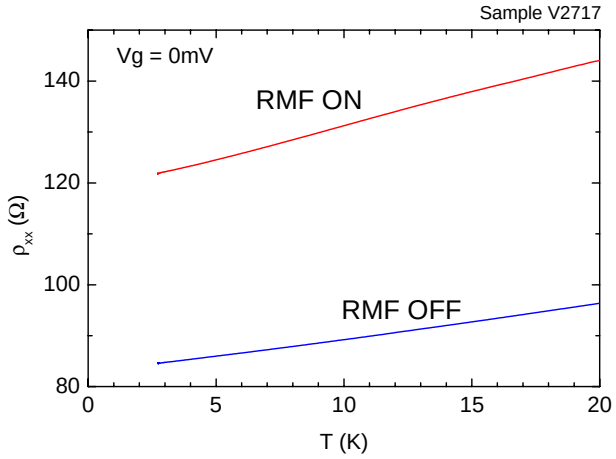

Figure 3.14: Temperature dependence of a RMF sample.

To see this, we plot the resistance increase $\Delta\rho$ from 2D MMF (including RMF) as a function of temperature T in Fig.3.15 (a). Those from 1D MMF are also shown as dotted lines for comparison. Though the resistivity increase, or the constant term A, are of the same order of magnitude, the temperature dependences are quite different. Note that the carrier density $n_e \approx 1.9\times10^{15}$ m^{-2}, mobility $\mu \approx 40$ m^2/Vs and the resistivity $\rho_0 \approx 90\,\Omega$ when the MMF are off are about the same for all the 2DES presented here. We fit the $\Delta\rho$ for 2D MMF with the same expression (3.5). The coefficients A, B, and C are summarized in Table 3.4. To see the qualitative difference between 1D and 2D modulation, we plotted in Fig.3.15 (b) the coefficient A of the T^2-term against the constant C term. It clearly tells that the T^2-term is absent or very small for 2D modulations.

The observation of T^2-term in random 1D MMF seemed to support the idea that any kind of modulation would lead to T^2-dependent resistivity component, but the absence of such term in 2D MMF (both regular and random) is in conflict with it.

*Different MMF profile is realized on the same sample by changing the azimuthal angle ϕ of the in-plane field $B_\parallel$. $\phi = 0°$ for V2718a and $\phi = 90°$ for V2718b.

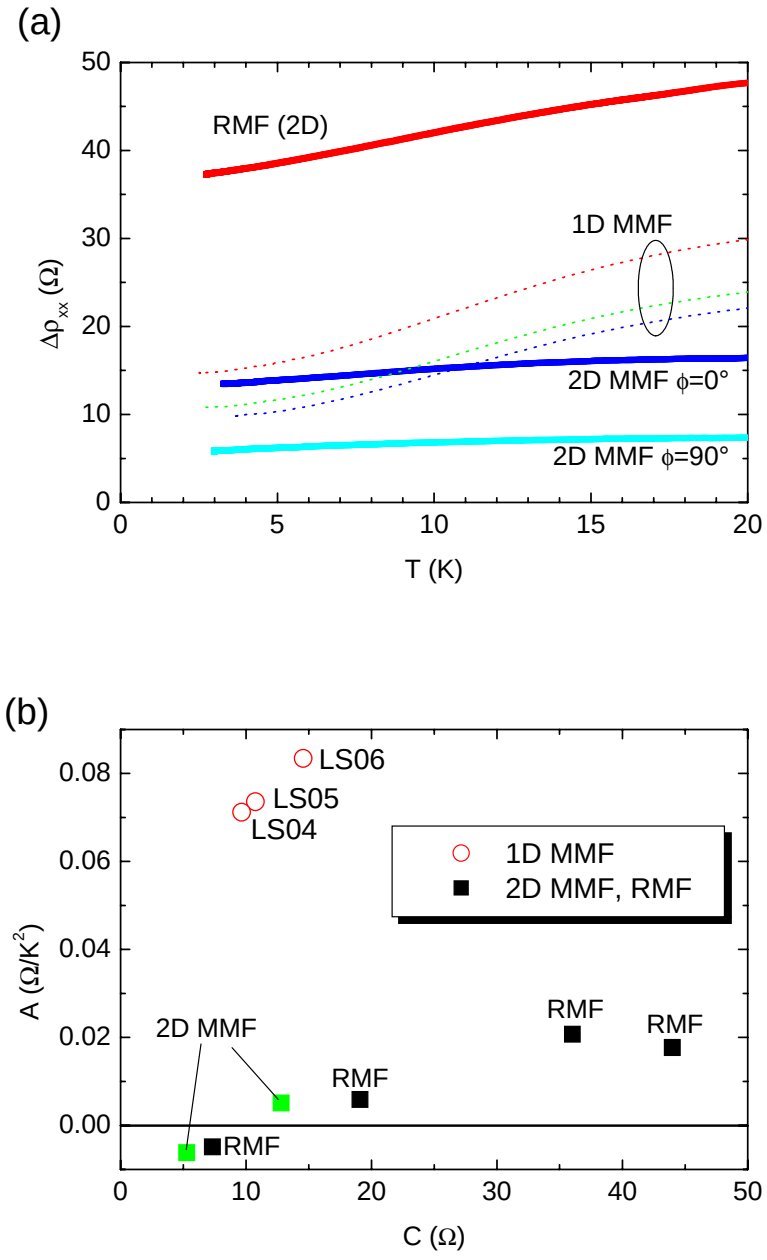

Figure 3.15: (a) Resistivity increase $\Delta\rho$ of 1D and 2D MMF as a function of temperature T. (b) Coefficient of T^2-term against constant term.

Table 3.4: Temperature dependence coefficient of the resistivity.

Sample	$n_e(\mathrm{m}^{-2})$	$\mu(\mathrm{m}^2/\mathrm{Vs})$	$A(\Omega/\mathrm{K}^2)$	$B(\Omega/\mathrm{K})$	$C(\Omega)$
V2717 RMF	1.833×10^{15}	39.8	0.021	0.403	36.02
V2707 RMF	1.991×10^{15}	32.2	0.018	0.570	43.99
V2710 RMF	1.956×10^{15}	34.3	0.006	0.272	19.09
V2709 RMF	1.887×10^{15}	37.2	-0.005	0.137	7.32
V2718a* 2DMMF	1.784×10^{15}	40.6	0.005	0.190	12.80
V2718b* 2DMMF	1.784×10^{15}	40.6	-0.006	0.215	5.27

For electrostatic modulations, T^2-term is also observed for 1D modulaton [18] but not for 2D modulations. Moreover, the random impurity responsible for a large part of the residual resistivity at low temperture does not give rise to the T^2-term. Therefore the T^2-term may be particular to 1D modulations. 1D modulations are modulations such that the anisotropy becomes maximum. Though our 2D MMF and RMF samples have some anisotropy it should be much smaller than the 1D MMF samples. It is possible that anisotropy plays an important role in the occurence of the T^2-term. But the reason for the qualitative difference in the temperature dependence is not clear at the moment and we hope a further progress of the theoretical investigation on this topic.

Chapter 4

Conclusion

In this thesis we studied the high-mobility semiconductor two-dimensional electron systems (2DES) in spatially modulated magnetic field (MMF), with special interest in random magnetic field (RMF). In order to produce MMFs in a controlled fashion, micropatterened film of non-hysteretic magnetic alloy, DyCu, was fabricated on 2DES Hall bars.

With the introduction of RMF, the resistance of the 2DES showed an increase with a quadratic dependence on the modulation amplitude. A cross-coil magnet system enabled us to study the magnetoresistance of a 2DES with fixed MMF component $\delta B(\boldsymbol{r})$ as a function of uniform field component $\bar{B}$. A 2DES with RMF showed a large positive magnetoresistance which look very similar to those observed around the half-filled Landau level state of unmodulated 2DES. This supports the idea of mapping composite fermion in random potential to electron in random magnetic field. Our data also suggests that the characteristic structure of the magnetoresistance curve is of classical nature associated to the cyclotron motion of electron. Analysis of Shubnikov-de Haas oscillation implies that the RMF does not significantly alter the electron effective mass and therefore is not likely to account for the reported mass enhancement of the composite fermion.

Introduction of randomness to one-dimensional MMF smears out the well-known commensurability oscillation in the magnetoresistance and changes it to a broad positive one, similar to that seen in two-dimensional RMF systems. However the temperature dependence of the resistance of 2DES with one-dimensional and two-dimensional MMF showed a qualitative difference that the T^2-dependent term observed in the former did not show up in the latter.

Acknowledgement

I would like to express my best gratitude and honor to my supervisor Prof. Y. Iye for the continual guidance and support and for the critical reading of this thesis. I am graterul to Prof. S. Katsumoto for valuable advice especially on experimental technique. I appreciate Dr. A. Endo, Dr. K. Kobayashi and M. Hirasawa for useful suggestions and discussions. I thank every person, present and in the past, at Iye-Katsumoto group and all my friends for sharing their valuable knowledge and time with me.

I learned much about one-dimensional modulation through the discussions with Dr. M. Kato and T. Sasaki. I am indebted Dr. T. Kawarabayashi for valuable discussions on random field.

I would like to dedicate this thesis to my parents, who continuously supported and encouraged me to pursue the study.

Finally I would like to thank for the financial supprot form the Japan Society for the Promotion of Science (JSPS).

References

[1] M.Ando, A.Endo, S.Katsumoto, Y. Iye, Physica B **284**, 1900 (2000).

[2] D. Weiss, K. von Klitzing, K. Ploog, and G. Weimann, EuroPhys. Lett. **8**, 179 (1989).

[3] R. R. Gerhards, D. Weiss, and K. von Klitzing, Phys. Rev. Lett. **62**, 1173 (1989).

[4] R. W. Winkler, J. P. Kotthaus, and K.Ploog, Phys. Rev. Lett. **62**, 1177 (1989).

[5] C. W. J. Beenakker, Phys. Rev. Lett. **62**, 2020 (1989).

[6] P. Vasilopoulus and F. M. Peeters, Phys. Rev. Lett. **63**, 2120 (1989).

[7] F. M. Peeters and P. Vasilopoulus, Phys. Rev. B **46**, 4667 (1992).

[8] D. P. Xue and G. Xiao, Phys. Rev. B **45**, 5986 (1992).

[9] F. M. Peeters and P. Vasilopoulus, Phys. Rev. B **47**, 1466 (1993).

[10] R. Yagi and Y. Iye, J. Phys. Soc. Jpn. **62**, 1279 (1993).

[11] S. Izawa, S. Katsumoto, A. Endo, and Y. Iye, J. Phys. Soc. Jpn. **64**, 706 (1995).

[12] H. A. Carmona, A. K. Geim, A. Nogaret, P. C. Main, T. J. Foster, M. Henini, S. P. Beaumont, and M. G. Blamire, Phys. Rev. Lett. **74**, 3009 (1995)

[13] P. D. Ye, D. Weiss, R. R. Gerhardts, M. Seeger, K. von Klitzing, K. Eberl, and H. Nickel, Phys. Rev. Lett. **74**, 3013 (1995).

[14] J. H. Davies and I. A. Larkin, Phys. Rev. B **49**, 4800 (1994), I. A. Larkin and J. H. Davies, A. R. Long, and R. Curso, Phys. Rev. B **56**, 15242 (1997), E. Skuras, A. R. Long, I. A. Larkin, J. H. Davies, and M. C. Holland, Appl. Phys. Lett. **70**, 871 (1997).

[15] A. Nogaret, S. Carlton, B. L. Gallagher, P. C. Main, M. Henini, R. Wirtz, R. Newbury, M. A. Howson, and S. P. Beaumont, Phys. Rev. B **55**, 16037 (1997).

[16] E. E. Mendez, P. J. Price, and M. Heiblum, Appl. Phys. Lett. **45**, 294 (1984).

[17] B. J. F. Lin, D. C. Tsui, and G. Weimann, Solid State Commun. **56**, 287 (1985).

[18] A. Messica, A. Soibel, U. Meirav, A. Stern, H. Shtrikman, V. Umansky, and D. Mahalu, Phys. Rev. Lett. **78**, 705 (1997).

[19] N. Overend, A. Nogaret, B. L. Gallagher, P. C. Main, R. Wirtz, R. Newbury, M. A. Howson, and S. P. Beaumont, Physica B **249-251**, 326 (1998).

[20] M. Kato, Thesis, University of Tokyo, Japan (2000) and references therein.

[21] T. Sasaki and F. Fukuyama, Unpublished.

[22] D. R. Hofstadter, Phys. Rev. B **14**,2239 (1976).

[23] D. Yoshioka and Y. Iye, J. Phys. Soc. Jpn. **56**, 2280 (1987).

[24] R. R. Gerhardts, D. Pfannkuche, and V. Gudmundsson, Phys. Rev. B **53**, 9591 (1996).

[25] M. C. Chang and M. F. Yang, Phys. Rev. B **57**, 13002 (1998).

[26] J. Yoshida, T. Ohtsuki, and Y. Ono, J. Phys. Soc. Jpn. **67**, 3886 (1998).

[27] P. D. Ye, D. Weiss, K. von Klitzing, K. Eberl, and H. Nickel, Appl. Phys. Lett. **67**, 1441 (1995).

[28] P. A. Lee and D. S. Fisher, Phys. Rev. Lett. **47**, 882 (1981)

[29] T. Sugiyama and N. Nagaosa, Phys. Rev. Lett. **70**, 1980 (1993), K. Yakubo and Y. Goto, Phys. Rev. B **54**, 13432 (1996), D. Z. Liu, X. C. Xie, S. Das Sarma, and S. C. Zhang, Phys. Rev. B **52**, 5858 (1995).

[30] Y. Avishai, Y. Hatsugai, and M. Kohmoto, Phys. Rev. B **47**, 9561 (1993), T. Kawarabayashi and T. Ohtsuki, Phys Rev. B **51**, 10897 (1995), D. N. Sheng and Z. Y. Weng, Phys. Rev. Lett. **75**, 2388 (1995), X. C. Xie, X. R. Wang, and D. Z. Liu, Phys. Rev. Lett. **80**, 3563 (1998), A. Furusaki, Phys. Rev. Lett. **82**, 604 (1999).

[31] V. Kalmeyer and S. C. Zhang, Phys. Rev. B **46**, 9889 (1992).

[32] V. Kalmeyer, D. Wei, D. P. Arovas, and S. C. Zhang, Phys. Rev. B **48**, 11095 (1993).

[33] D. V. Khveshchenko, Phys. Rev. Lett. **77**, 362 (1996), A. D. Mirlin and P. Wölfle, Phys. Rev. B **55**, 5141 (1997), N. Nagaosa and H. Fukuyama, J. Phys. Soc. Jpn. **67**, 3353 (1998).

[34] N. Nagaosa and P. A. Lee, Phys. Rev. Lett. **64**, 2450 (1990).

[35] R. B. Laughlin, Phys. Rev. Lett. **50**, 1395 (1983).

[36] J. K. Jain, Phys. Rev. B **41**, 7653 (1990).

[37] H. W. Jiang, H. L. Stormer, D. C. Tsui, L. N. Pfeiffer, and K. W. West, Phys. Rev. B **40**, 12013 (1989).

[38] R. R. Du, H. L. Stormer, D. C. Tsui, A. S. Yeh, L. N. Pffeifer, and K. W. West, Phys. Rev. Lett. **70**, 2944 (1993).

[39] R. R. Du, H. L. Stormer, D. C. Tsui, L. N. Pffeifer, and K. W. West, Phys. Rev. Lett. **73**, 3274 (1994).

[40] B. I. Halperin, P. A. Lee, and N. Read, Phys. Rev. B **47**, 7312 (1993).

[41] J. Rammer and A. L. Shalenkov, Phys. Rev. B **36**, 3135 (1987).

[42] A. G. Aronov, A. D. Mirlin, and P. Wölfle, Phys. Rev. B **49**, 16609 (1994), A. G. Aronov, E. Altshuler, A. D. Mirlin, and P. Wölfle, Europhys. Lett. **29**, 239 (1995).

[43] A. D. Mirlin, J. Wilke, F. Evers, D. G. Polyakov, and P Wölfle, Phys. Rev. Lett. **83**, 2801 (1999), A. D. Mirlin, D. G. Polyakov, and P. Wölfle, Phys. Rev. Lett. **80**, 2429 (1998), F. Evers, A. D. Mirlin, D. G. Polyakov, and P. Wölfle, Phys. Rev. B **60**, 8951 (1999).

[44] D. V. Khveshchenko, Phys. Rev. Lett. **77**, 1817 (1996).

[45] P. Hedegård and Anders Smith, Phys. Rev. B **51**, 10869 (1995).

[46] A. K. Geim, S. J. Bending, I. V. Gigorieva, and M. G. Blamire, Phys. Rev. B **49**, 5749 (1994).

[47] A. Smith, R. Taboryski, L. T. Hansen, C. B. Sørensen, P. Hedegård, and P. E. Lindelof, Phys. Rev. B **50**, 14726 (1994).

[48] F. B. Mancoff, R. M. Clarke, C. M. Marcus, S. C. Zhang, K. Campman, and A. C. Gossard, Phys. Rev. B **51**, 13269 (1995).

[49] F. B. Mancoff, L. J. Zielinski, C. M. Marcus, K. Campman, and A. C. Gossard, Phys. Rev. B **53**, 7599 (1996).

[50] G. M. Gusev, U. Gennser, X. Kleber, D. K. Maude, J. C. Portal, D. I. Lubyshev, P. Basmaji, M. de P. A. Silva, J. C. Rossi, and Yu. V. Nastaushev, Phys. Rev. B **53**, 13641 (1996).

[51] P. D. Ye, Unpublished.

[52] R. B. Dingle, Proc. R. Soc. London Sect. A **211**, 517 (1952).

[53] T. Ando, J. Phys. Soc. Jpn. **37**, 1233 (1974).